Beam shape control using shape memory alloys

Kelly, Brian L.

Monterey, California. Naval Postgraduate School

NAVAL POSTGRADUATE SCHOOL
Monterey, California

THESIS

BEAM SHAPE CONTROL USING SHAPE MEMORY ALLOYS

by

Brian L. Kelly

December 1998

Thesis Advisor: Brij N. Agrawal
Co-Advisor: Gangbing Song

Approved for public release; distribution is unlimited

REPORT DOCUMENTATION PAGE

Form Approved
OMB No. 0704-0188

1. AGENCY USE ONLY *(Leave blank)*	2. REPORT DATE	3. REPORT TYPE AND DATES COVERED
	December 1998	Master's Thesis

4. TITLE AND SUBTITLE
BEAM SHAPE CONTROL USING SHAPE MEMORY ALLOYS

5. FUNDING NUMBERS

6. AUTHOR(S)
Kelly, Brian L.

7. PERFORMING ORGANIZATION NAME(S) AND ADDRESS(ES)
Naval Postgraduate School
Monterey, CA 93943-5000

8. PERFORMING ORGANIZATION REPORT NUMBER

9. SPONSORING / MONITORING AGENCY NAME(S) AND ADDRESS(ES)

10. SPONSORING / MONITORING AGENCY REPORT NUMBER

11. SUPPLEMENTARY NOTES
The views expressed in this thesis are those of the author and do not reflect the official policy or position of the Department of Defense or the U.S. Government.

12a. DISTRIBUTION / AVAILABILITY STATEMENT
Approved for public release; distribution is unlimited.

12b. DISTRIBUTION CODE

13. ABSTRACT *(maximum 200 words)*

This thesis presents the design and experimental results of active position control of a shape memory alloy (SMA) wire and a SMA wire actuated composite beam. The wire is a single SMA Nickel Titanium wire mounted on a single wire test stand. The composite beam is Aluminum honeycomb with SMA wires embedded in one of its face sheets for active shape control. The potential applications of this experiment include thermo-distortion compensation for precision space structures, stern shape control for submarines, and flap shape control for aeronautical applications. SMA wires are chosen as actuating elements due to their high recovery stress (> 700 MPa) and its tolerance to high strain (up to 8 %). SMA wires are inherently nonlinear, which poses a challenge for control design. The experimental setup consists of the single wire test stand and the composite beam with embedded SMA wires, a HP programmable power supply, a Linear Variable Differential Transformer (LVDT), an infrared laser range sensor, and a dSpace system with a Texas Instrument C-30 DSP for data acquisition and real-time control. A Position and Derivative (PD) control with feed forward action was designed and implemented, and a control accuracy of 0.1 mm was achieved. A non-linear control was added which gives a control accuracy of 0.05 mm with a much faster response.

14. SUBJECT TERMS	15. NUMBER OF PAGES
Controls, active damping, shape memory alloys, vibration control, shape control, Nitinol.	76
	16. PRICE CODE

17. SECURITY CLASSIFICATION OF REPORT	18. SECURITY CLASSIFICATION OF THIS PAGE	19. SECURITY CLASSIFI- CATION OF ABSTRACT	20. LIMITATION OF ABSTRACT
Unclassified	Unclassified	Unclassified	UL

NSN 7540-01-280-5500

Standard Form 298 (Rev. 2-89)
Prescribed by ANSI Std. 239-18

Approved for public release; distribution is unlimited

BEAM SHAPE CONTROL USING SHAPE MEMORY ALLOYS

Brian L. Kelly
Lieutenant, United States Navy
B.S.E.E., University of South Carolina, 1993

Submitted in partial fulfillment of the
requirements for the degree of

MASTER OF SCIENCE IN ASTRONAUTICAL ENGINEERING

from the

NAVAL POSTGRADUATE SCHOOL
December 1998

Author: [redacted]
Brian L. Kelly

Approved by: [redacted]
Brij N. Agrawal, Thesis Advisor

[redacted]
Gangbing Song, Co-Advisor

[redacted]
G. Lindsey, Chairman
Department of Aeronautics and Astronautics

ABSTRACT

This thesis presents the design and experimental results of active position control of a shape memory alloy (SMA) wire and a SMA wire actuated composite beam. The wire is a single SMA Nickel Titanium wire mounted on a single wire test stand. The composite beam is Aluminum honeycomb with SMA wires embedded in one of its face sheets for active shape control. The potential applications of this experiment include thermo-distortion compensation for precision space structures, stern shape control for submarines, and flap shape control for aeronautical applications. SMA wires are chosen as actuating elements due to their high recovery stress (> 700 MPa) and its tolerance to high strain (up to 8 %). SMA wires are inherently nonlinear, which poses a challenge for control design. The experimental setup consists of the single wire test stand and the composite beam with embedded SMA wires, a HP programmable power supply, a Linear Variable Differential Transformer (LVDT), an infrared laser range sensor, and a dSpace system with a Texas Instrument C-30 DSP for data acquisition and real-time control. A Position and Derivative (PD) control with feed forward action was designed and implemented, and a control accuracy of 0.1 mm was achieved. A non-linear control was added which gives a control accuracy of 0.05 mm with a much faster response.

TABLE OF CONTENTS

LIST OF FIGURES

LIST OF TABLES

LIST OF ABBREVIATIONS

A_f	Reverse Transformation Finish Temperature
Al	Aluminum
A_s	Reverse Transformation Start Temperature
Cu	Copper
DC	Direct Current
HP	Hewlett Packard
LVDT	Linear Variable Differential Transformer
M_d	Martensite Limiting Upper Temperature
M_f	Martensite Finish Temperature
MPa	Mega Pascals
M_s	Martensite Start Temperature
Ni	Nickel
PID	Proportional-Integral-Derivative
PD	Proportional-Derivative
SMA	Shape Memory Alloy
SRDC	Spacecraft Research and Design Center
Ti	Titanium
Tanh	Hyperbolic Tangent
Zn	Zinc

ACKNOWLEDGEMENT

There are several individuals whom I would like to thank for their assistance in the completion of my thesis. First I would like to thank Dr. Suraj Rawal and Dr. Bernie Carpenter of Lockheed Martin, Denver, Colorado, for allowing me to use their lab and teaching me the fundamentals of Shape Memory Alloys. I would like to thank the Mechanical Engineering Department machine shop for their timely machining of the necessary parts to build the experimental apparatus. I would especially like to thank Dr. Gangbing Song for his guidance and motivation through the tough times. Also, thanks to Prof. Brij Agrawal for his expert guidance and support throughout the thesis process.

Finally, I would like to thank my family for putting up with me during this time. Without their support, this thesis would not have been possible.

I. INTRODUCTION

A. BACKGROUND

New spacecraft designs, including space based lasers, and space based radar are being designed with stringent structural requirements for dimensional stability, and pointing accuracy. As space structures become larger and pointing accuracy requirements become higher, the need for precision active shape control becomes increasingly important. To meet these challenges, "smart structures" need to be investigated. A smart structure employs distributed actuators and sensors, and one or more microprocessors that analyze the responses from the sensors and use distributed-parameter control theory to command the actuators to apply localized strains to insure the system responds in a desired fashion. A smart structure has the capability to respond to a changing external environment (such as mechanical or thermal loads) as well as to a changing internal environment (such as damage or failure). Smart actuators are used to alter system response, such as stiffness, damping and shape in a controlled manner. Much of the early development of smart structure technology was driven by space applications, such as vibration and shape control of large flexible space structures. Now smart structure research has been extended to aeronautical and other systems. Shape memory alloys, due to their capability of large actuation forces and displacements, have become promising candidates and have been proposed for use in a wide array of engineering structures. These include antenna shape control, submarine control surfaces, flap shape control and helicopter tail rotor shafts for aeronautical applications.

Shape memory alloys are the newest members of a family of smart materials. The smart materials include piezo-ceramics, electro-strictors, electro-rheological fluids, paraffin wax and others. Shape memory alloys undergo a heat activated reversible crystalline phase transformation. In particular, Nitinol (a Nickel Titanium intermetallic discovered by the then Naval Ordinance Laboratory in 1963) has provided attractive engineering properties for use in lightweight actuator designs and adaptive composite structures. The ability of shape memory alloys to generate high recovery stresses over large strains provides motivation for assessing the feasibility of their use in applications

for active spacecraft shape and vibration control. Compared to piezo-ceramic and proof-mass actuators, shape memory actuators may offer substantial advantages for certain types of applications.

Shape memory alloys can be cycled millions of times over large strains (> 3%) and at high stress levels (> 50 ksi or 350 MPa), providing 30 to 40 times the mechanical transductance of piezo-ceramics. In addition, the use of SMAs can provide a volume and weight efficient approach for generating stresses to deform and control the shape of precision structures. Moreover, the hysteretic nature of these materials may provide supplemental, passive damping when incorporated in active structural elements of smart structures.

Shape memory alloys are difficult to model due to their non-linearity. Without proper modeling of SMA behavior, credible actuator design efforts, which attempt to exploit the high transductance of SMA's, is extremely challenging. Additionally, the temperature hysteresis of SMA's will present additional control problems for spacecraft structures, which go through large temperature variations.

B. SCOPE OF THESIS

This thesis examines the feasibility of using shape memory alloy for antenna shape control. This is the first attempt to study shape memory alloys in the Spacecraft Research and Design Center at the Naval Postgraduate School. The shape memory alloy experiment had to be developed and made operational at the SRDC. Once operational, simple control systems were designed for a single shape memory wire and a shape memory composite beam. The control design used proportional plus derivative control, which provided control accuracy to 0.1 mm. Although this control design accuracy is very good, the response times were very slow. A non-linear control was then added which greatly improved both the response times and the accuracy.

The remainder of this thesis is organized as follows. Section II describes the properties of shape memory alloys; Section III describes the experimental setup. Section IV describes the control system design of the single wire. Section V describes the control

system design of the shape memory composite beam. Section VI discusses the conclusions and further research possibilities.

II. PROPERTIES OF SHAPE MEMORY ALLOY

A. SHAPE MEMORY EFFECT

The shape memory effect is a unique property of certain alloys exhibiting martensitic transformations. These materials can be deformed in the low temperature phase, and they will recover their original shape by the reverse transformation upon heating to a critical temperature called the reverse transformation temperature. This shape change is due to a change in the atomic crystalline structure of the alloy. Figure 1 shows an example of heating of a wire. Force is applied to the wire to deform it while it is cool. With the force removed, the wire remains deformed until heated. Once heated,

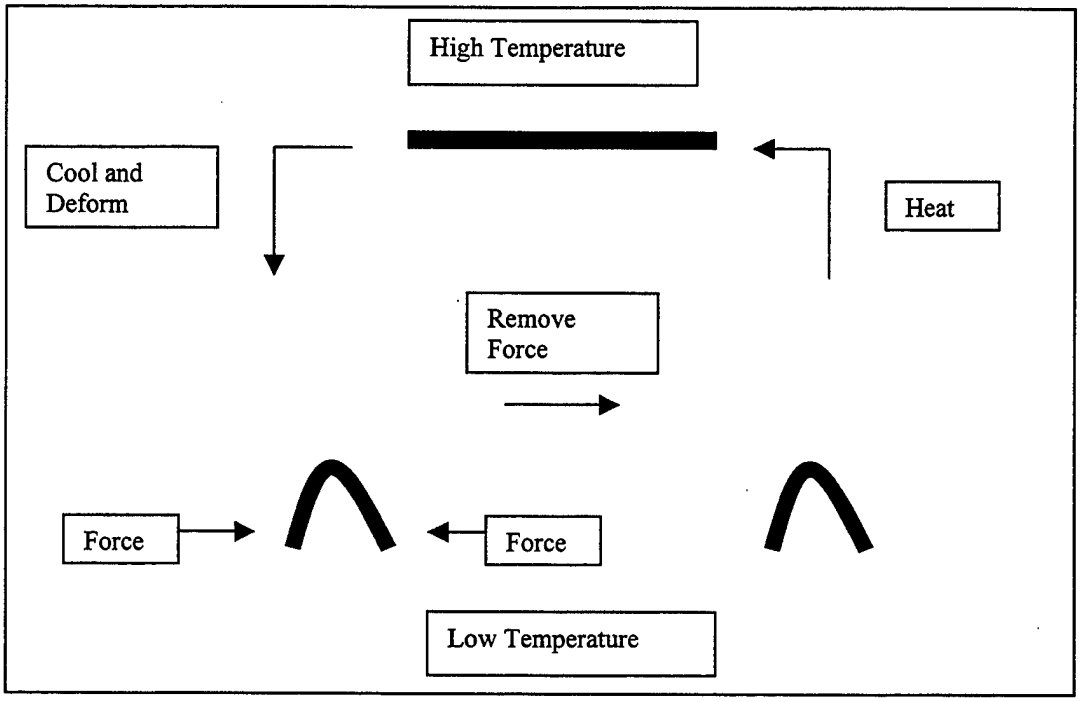

Figure 1: Bending of a shape memory wire

the wire returns to its original shape. This is referred to as the one-way shape memory effect. The high temperature crystal structure is called austenite and is cubic. When cooled, the material transforms to a structure called martensite with a monoclinic lattice structure, which looks like a parallelogram in two dimensions (Figure 2).

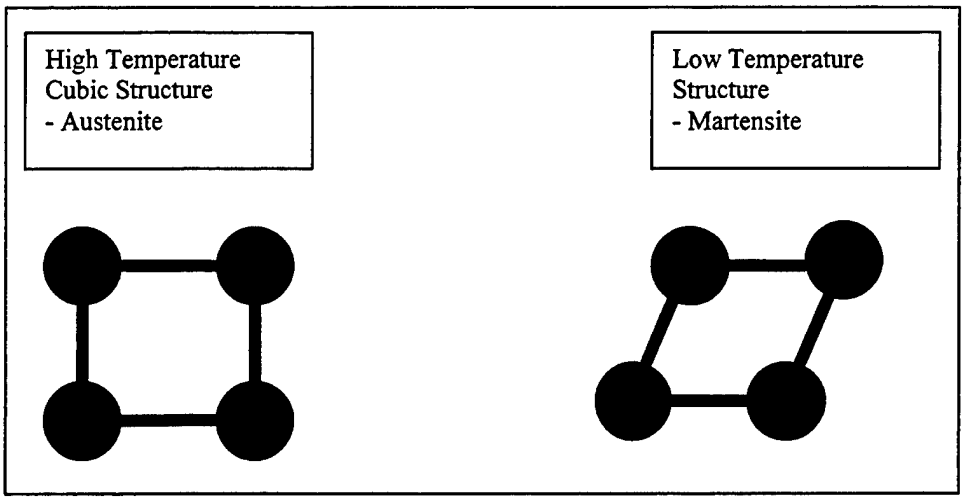

Figure 2: Nickel titanium shape memory alloy crystal structures

When a piece of shape memory material containing many atoms is cooled, the atoms do not all tilt in the same direction. Instead, alternating rows of atoms tilting either left or right are formed (Figure 3). Any four atoms in the low temperature structure have the martensite parallelogram shape.

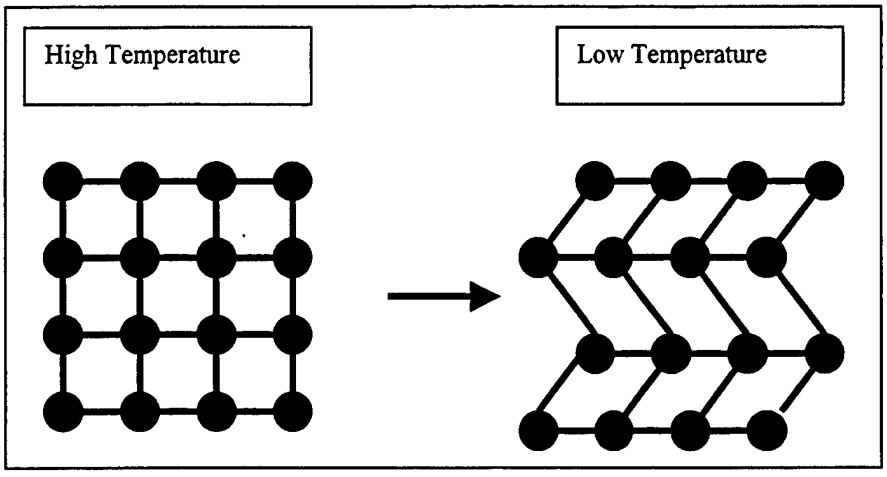

Figure 3: Shape memory alloy atomic rearrangement upon cooling

The alternating rows in Figure 3 is called twinning, because the atoms form mirror images of themselves, or twins, through a plane of symmetry. When a stress is applied to the material it will deform, or accumulate strain, as the twins are reoriented so they all lie in the same direction. This is shown in Figure 4. This is called de-twinning, and in shape memory alloys, the stress required to reorient twins is relatively low.

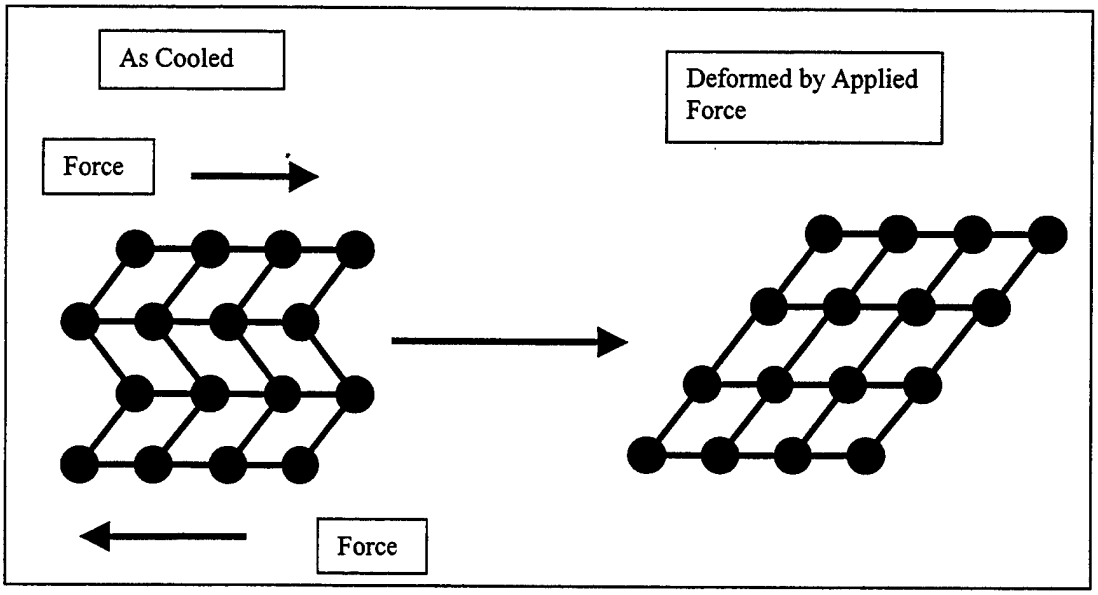

Figure 4: Deformation of low temperature structure by applied force

Heating the material will cause the deformed martensite to revert to austenite and the original shape of the piece will be obtained. This occurs because the original atomic positions are always maintained in the austenite phase. Additionally, a temperature hysteresis occurs due to processes that take place on an atomic scale. In other words the austenite to martensite transformation occurs over a lower temperature range than the martensite to austenite transformation. The absolute values of the transformation temperatures, and the hysteresis width and shape all depend largely on alloy composition and processing. Most shape memory alloys have a hysteresis loop width of 10 – 50° C. The hysteresis is due to the internal friction caused by the movement of the austenite to martensite interface, and by the creation of structural defects within the alloy crystal structure. Figure 5 shows a typical temperature hysteresis. At a temperature below M_f (martensite finish temperature) the material is 100% martensite. As it is heated it will

reach a temperature A_s (reverse transformation start temperature) which is the point that austenite just begins to form. Further heating will cause the material will convert to 100% austenite at A_f (reverse transformation finish temperature). If the material is then cooled, martensite will begin to form at M_s (martensite start temperature) and will be 100% martensite at M_f. This hysteresis makes control of SMA materials very difficult.

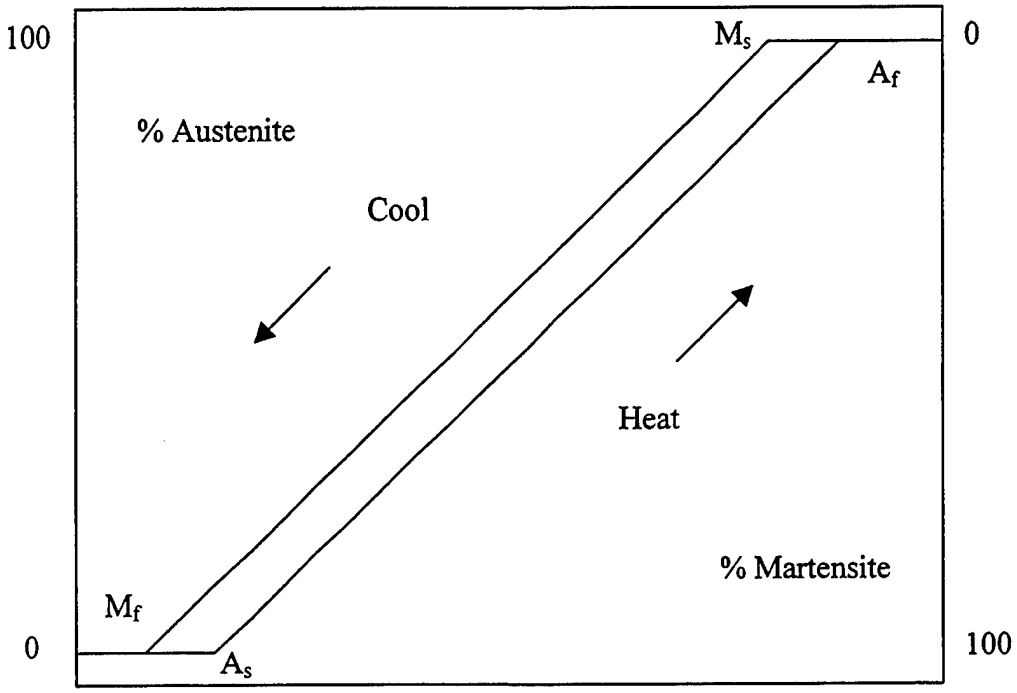

Figure 5. Temperature hysteresis

1. Two-Way Shape Memory Effect

The one-way shape memory effect requires a force to deform the material while it is cool, but will recover its shape when heated. A two-way effect can be obtained, where the shape memory material will return to a low temperature shape on cooling, as well as to a high temperature shape on heating. This behavior is referred to as the two-way shape memory effect. In both the one-way and two-way shape memory effects, only during heating work can be generated. During cooling with the two-way effect, the material simply recovers its low temperature shape and cannot provide a force to external

mechanical components. There are five basic processing techniques which can be used to impart the two-way effect to a shape memory alloy element:

- Highly deform the element in the martensitic state.
- Deform the element in the austenitic state with a stress that is greater than the minimum stress that causes the material to yield.
- Deform the element in the austenitic state by some applied force, then lower the temperature below 100% martensitic state for a long period, maintaining the applied force all the time.
- Constrain the element in the martensitic state and then heat it until it transforms to the austenitic state.
- Deform the element after aging has caused the formation of small precipitates in the austenitic state.

All of these techniques introduce internal stress sites such as dislocations, stable martensite (martensite which will not revert to austenite when heated), or minute precipitates. The stress sites serve to control the direction in which the martensite twins orient themselves during cooling. That is, there is a preferred orientation on the atomic scale, which causes the shape memory element to assume the required low temperature macroscopic shape, upon cooling (Ref 6).

2. All-Around Shape Memory Effect

Finally, there is an all-around shape memory effect. The all-around shape memory effect differs from the two-way effect in two ways. First, a greater amount of shape change is possible with the all-around effect. Second, the high and low temperature shapes are exact inverses of each other; i.e. a complete reversal of curvature is possible in the case of a piece of shape memory strip (Figure 6). It is possible to impart the all-around effect in an alloy with composition of Ti/50.5 atomic percentage Ni by constraining the material to its high temperature shape and aging at a temperature of 400 °C for 50 hours. The all-around shape memory effect is not usually used in applications to provide motion in the reverse direction because of the extra processing involved and a

lack of reliability. Instead, some outside biasing force is used to deform the shape memory element at low temperature and any two-way effect that is present helps to reduce the amount of biasing force needed for this.

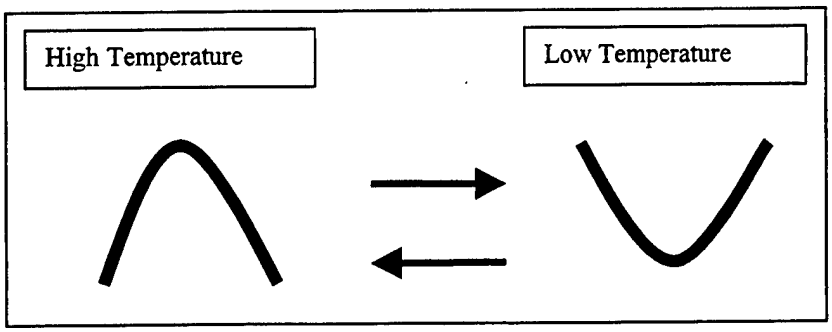

Figure 6: All-around shape memory effect

B. ALLOY TYPES

There are many known alloy systems which exhibit the shape memory effect, but only three have shown promise for commercial applications. They are Nickel-Titanium (Ni-Ti), Copper-Zinc-Aluminum (Cu-Zn-Al), and Copper-Aluminum-Nickel (Cu-Al-Ni).

The nickel titanium alloys (Nitinol) have typical compositions of approximately 50 atomic percentage Ni / 50 atomic percentage Ti, and may have small additions of copper, iron, cobalt, or chromium. Nickel-titanium is about four times the cost of Cu-Zn-Al alloys, but it has several advantages over Cu-Zn-Al and Cu-Al-Ni: greater ductility, more recoverable motion, excellent corrosion resistance (comparable to series 300 stainless steels), stable transformation temperatures, high biocompatability, and the ability to be electrically heated for shape recovery.

The copper-zinc-aluminum alloys have a typical composition of 15 – 25 weight percentage Zn / 6 – 9 weight percentage Al / balance Cu. Cu-Zn-Al alloys are lower in cost than nickel titanium, but they possess some inferior characteristics. Transformation temperatures can drift slightly during cycling (particularly at service temperatures greater than 100 °C) and to a significant extent if the alloy is not processed properly. These

alloys are susceptible to stress corrosion cracking when exposed to certain corrosive agents.

The copper-aluminum-nickel alloys have a typical composition of 13 – 14 weight percentage Al / 3 – 4 weight percentage Ni / balance Cu. Cu-Al-Ni alloys possess lower ductility than either Ni-Ti or Cu-Zn-Al. Their corrosion resistance is inferior to Ni-Ti and their cost is higher than Cu-Zn-Al. Cu-Al-Ni alloys undergo less degradation in shape memory properties than Cu-Zn-Al, after exposure to temperatures in the 100 to 350^{O} C range. In addition, Cu-Al-Ni alloys have the highest transformation temperatures of the three alloys.

C. MECHANICAL BEHAVIOR

1. Types of Motion

Strain accumulation results from the cooling and deforming shape memory material. When the material is heated the strain is relieved as the atoms shift back to their high temperature positions. Therefore, a shape memory wire bent at low temperature becomes straight when heated. Shape memory alloys can be used for linear motion and for torsion as well as bending.

2. Amount of Motion

The amount of motion that can be obtained from a shape memory component is limited by the amount that the atoms move when they reposition themselves from the low temperature deformed structure to the high temperature cubic structure. This amount differs for different alloys. For nickel titanium, the maximum motion is 8%. For example, a 30-cm long nickel titanium wire can provide a motion of 2.4 cm. If a nickel titanium shape memory element is allowed to recover its high temperature shape free of external forces, then the 8% motion can probably be achieved multiple times. However,

if significant external forces are applied to the same element during shape recovery, then the motion obtained over repeated cycles will be less than 8%.

D. STRESS-STRAIN BEHAVIOR

Shape memory alloys show a marked temperature dependence, because of the reversible austenite to martensite transformation. Figure 7 shows the stress-strain behavior of a shape memory alloy at or below the M_f temperature.

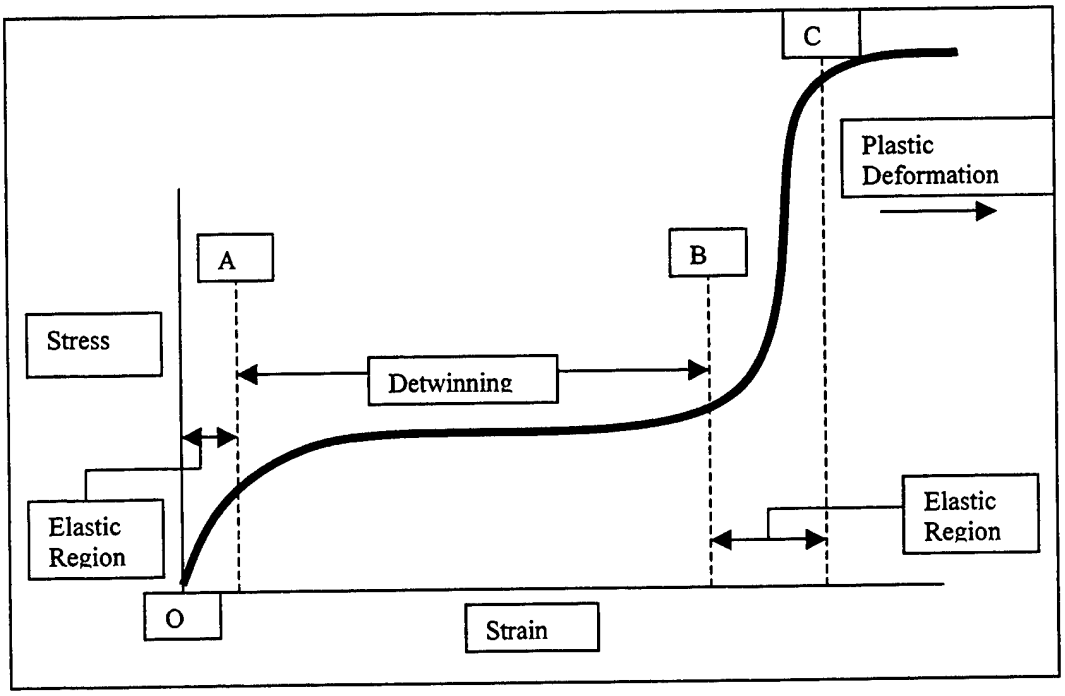

Figure 7. Stress-strain behavior at or below M_f

The microstructure consists of randomly oriented martensite twins, the initial curve segment OA represents elastic deformation until the stress level is sufficient to start the twins to reorient according to the applied stress field, at point A. In the segment AB the twins reorient until they all lie in the same crystallographic direction. This process is known as detwinning. Detwinning is complete at point B, and the martensite undergoes mostly elastic deformation again in segment BC. At point C the stress level is sufficient

to start plastic deformation of the martensite. The shape memory effect is destroyed or severely diminished by plastic deformation of the martensite past point C.

The stress-strain behavior of a shape memory alloy at a temperature above A_f, and below the M_d temperature (the material is fully austenitic) is shown in Figure 8. The M_d temperature is limiting upper temperature to the formation of stress induced martensite. The initial curve segment up to point A represents only elastic deformation. At point A, martensite begins to form from the austenite. This material is referred to as stress induced martensite. In the curve segment AB the austenite matrix is converted to martensite with a homogeneous crystographic orientation. Segment BC represents elastic deformation, with plastic deformation occurring after point C. For the unloading behavior of shape memory alloys at temperatures between A_f and M_d. Stress-strain curves at still higher temperatures are similar to that shown in Figure 8, except that the stress level at which the stress induced martensite forms is higher (it increases in a linear fashion with increasing temperature).

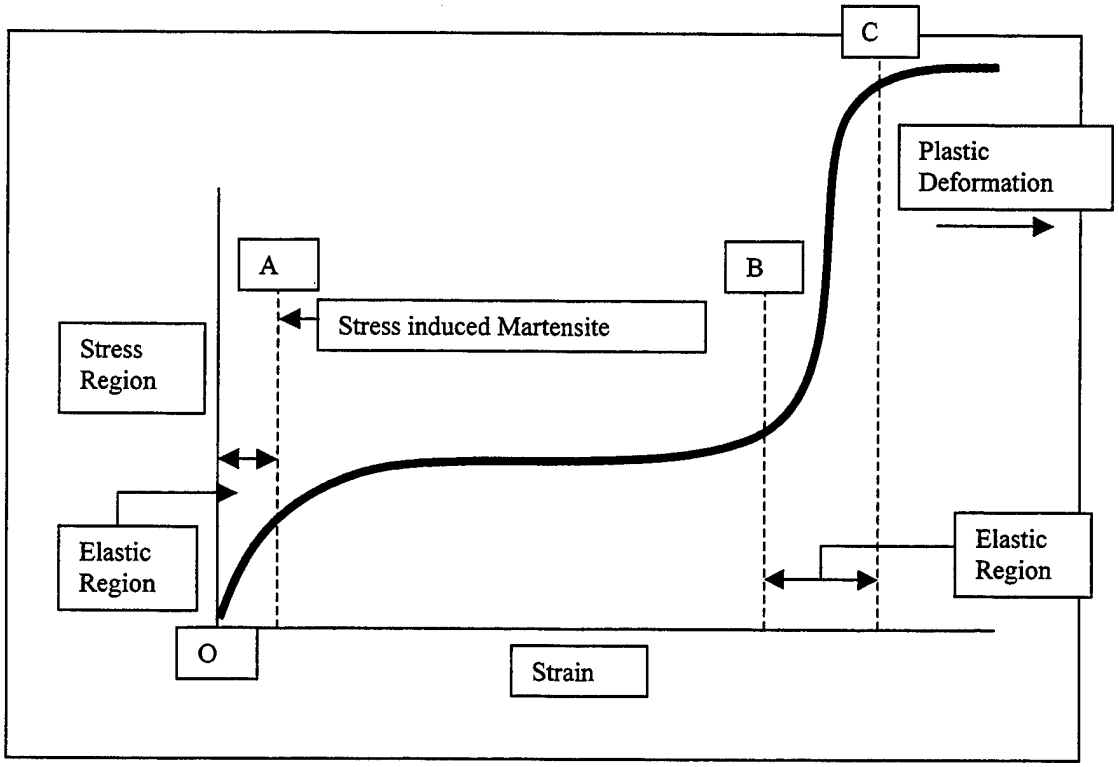

Figure 8. Stress-strain above A_f and below M_d

At temperatures above M_d, non-elastic deformation is entirely due to plastic yielding, and no stress induced martensite is formed. Figure 9 shows the stress-strain curve of a shape memory alloy just above the M_d temperature.

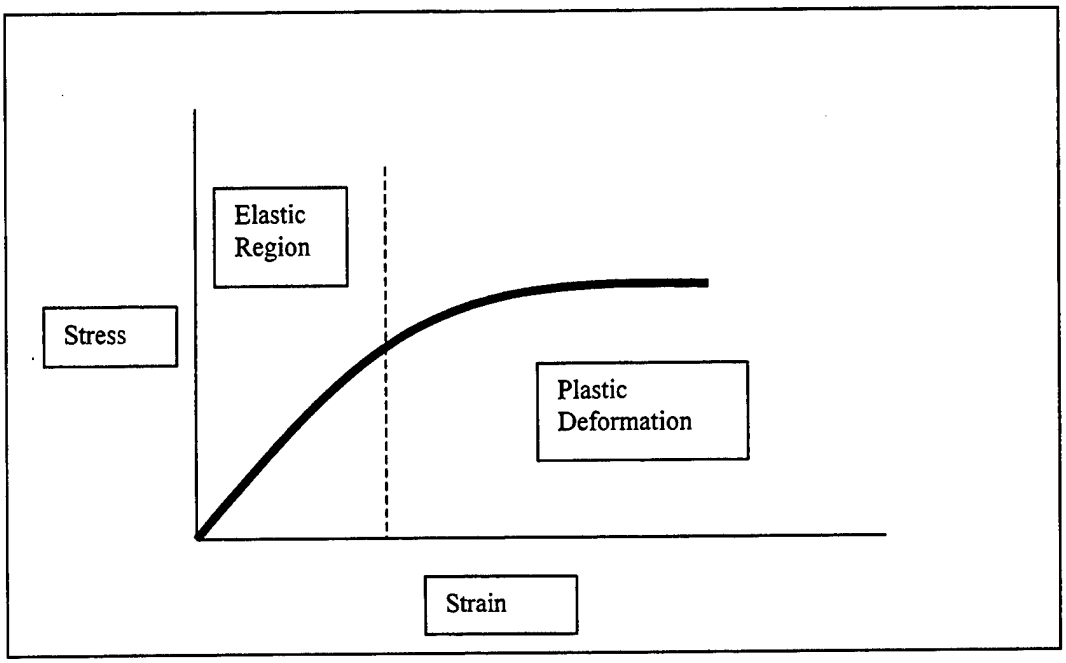

Figure 9. Stress-strain behavior above the M_d temperature

E. APPLICATIONS OF SHAPE MEMORY ALLOY'S

Shape memory alloys have many unique properties which lend themselves to a variety of applications. Large heat recoverable strains of up to 8% are obtained in NiTi alloys over a relatively narrow temperature range. If a NiTi alloy is constrained to prevent the shape memory effect from occurring, then stresses of up to 700 MPa can be generated.

The first large scale application of SMA's was as a coupling to connect titanium hydraulic tubing in the Grumman F-14 aircraft. The second major application of SMA's was their use in electrical connectors. SMA's are now being used for precision space structures, stern shape control for submarines and for flap shape control for aeronautical applications.

F.PROPERTIES OF NICKEL TITANIUM ALLOY

Table 1 lists the shape memory properties of nickel titanium.

Transformation Properties	
Transformation Temperature	-200 to 110 °C
Latent Heat of Transformation	5.78 cal/g
Transformation Strain (for polycrystalline material)	
For a single cycle	8% maximum
For 100 cycles	6%
For 100000 cycles	4%
Hysteresis	30 to 50 °C
Physical Properties	
Melting Point	1300 °C
Density	6.45 g/cm^3
Thermal Conductivity	
Austenite	0.18 W/cm°C
Martensite	0.086 W/cm°C
Specific Heat	0.20 cal/g °C
Corrosion Performance	Excellent
Electrical Properties	
Resistivity (ρ)	
[resistance = ρ x length/cross-sectional area]	
Austenite	~100 μΩ cm
Martensite	~80 μΩ cm
Magnetic Permeability	< 1.002
Magnetic Susceptibility	3.0 x 10^6 emu/g
Mechanical Properties	
Young's Modulus	
Austenite	~83 Gpa
Matensite	~28 – 41 Gpa
Yield Strength	
Austenite	195 – 690 MPa
Matensite	70 – 140 MPa
Ultimate Tensile Strength	
Fully annealed	895 MPa
Work hardened	1900 MPa
Poisson's Ratio	0.33
Elongation at Failure	
Fully annealed	25 – 50%
Work hardened	5 – 10%
Hot Workability	Quite good
Cold Workability	Difficult
Machinability	Difficult

Table 1. Properties of Nickel Titanium Shape Memory Alloy

III. THE NPS SHAPE MEMORY ALLOY EXPERIMENT

The initial goals of the NPS shape memory alloy experiment were first to demonstrate a simple control system for a single shape memory wire, and secondly to demonstrate a simple control system for the shape memory composite beam.

A. EXPERIMENTAL SETUP

1. Single Wire Experiment

The initial experiment was performed using a single wire in order to gain experience and confidence prior to experimenting with the shape memory composite beam. A block diagram of the single wire experiment is shown in Figure 10. A Nickel-Titanium shape memory alloy wire (30.48 cm in length and 0.381 mm in diameter) was mounted to a single wire test stand that allows for movement in the wire. A control system was designed using MATLAB/ Simulink. dSPACE Data Acquisition and Real Time Control system is used to interface the software to the hardware. An output voltage, which was proportional to the desired current, was sent to a Hewlett Packard programmable power supply. The power supply then delivered a direct current to the shape memory wire, which serves to heat the wire. The heating of the wire results in a phase transformation, which was seen as a shrinking of the wire. A linear variable differential transformer (LVDT) was used to measure the wire displacement. This displacement was then feed back to the dSpace interface. Additionally, a Hewlett Packard oscilloscope was used to display both the output voltage from dSpace, and the displacement voltage output from the LVDT. The actual experiment is pictured in Figure 11.

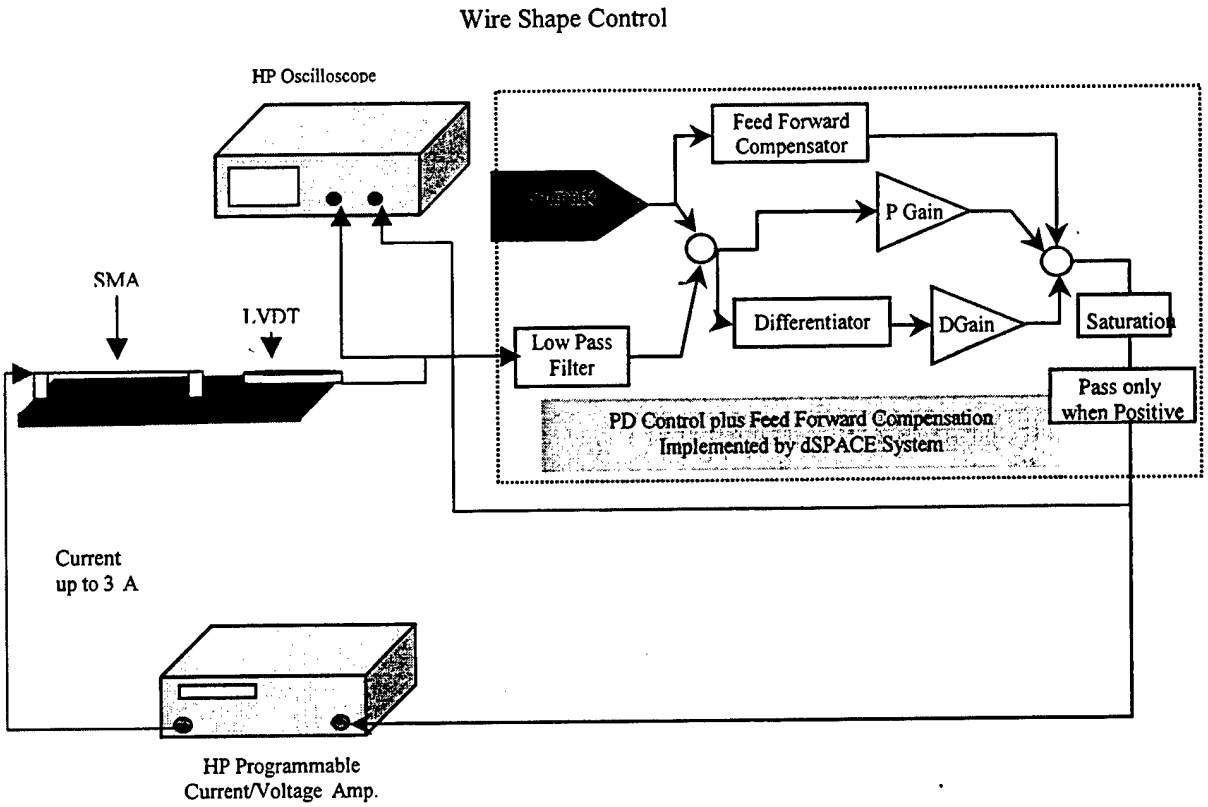

Figure 10. Single wire experiment block diagram

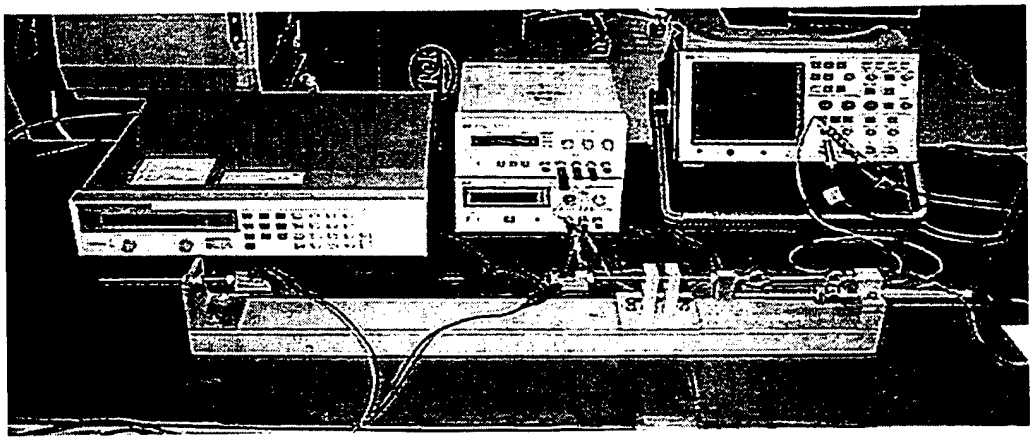

Figure 11. Single wire experiment

2. Shape Memory Alloy Beam Experiment

A block diagram of the shape memory alloy beam experiment is shown in Figure 12. The setup is similar to the single wire experiment in terms of the equipment used. The same HP programmable power supply was used to deliver direct current to the shape memory beam. The MATLAB/Simulink was used to design the control system, and dSpace was used to interface the software with the hardware. As the shape memory wire was heated, the beam deformed. A laser sensor was used to measure the displacement of the beam tip. Again, a HP oscilloscope is used to display both the output voltage from dSpace and the displacement output voltage from the laser sensor. The actual experiment is pictured in Figure 13.

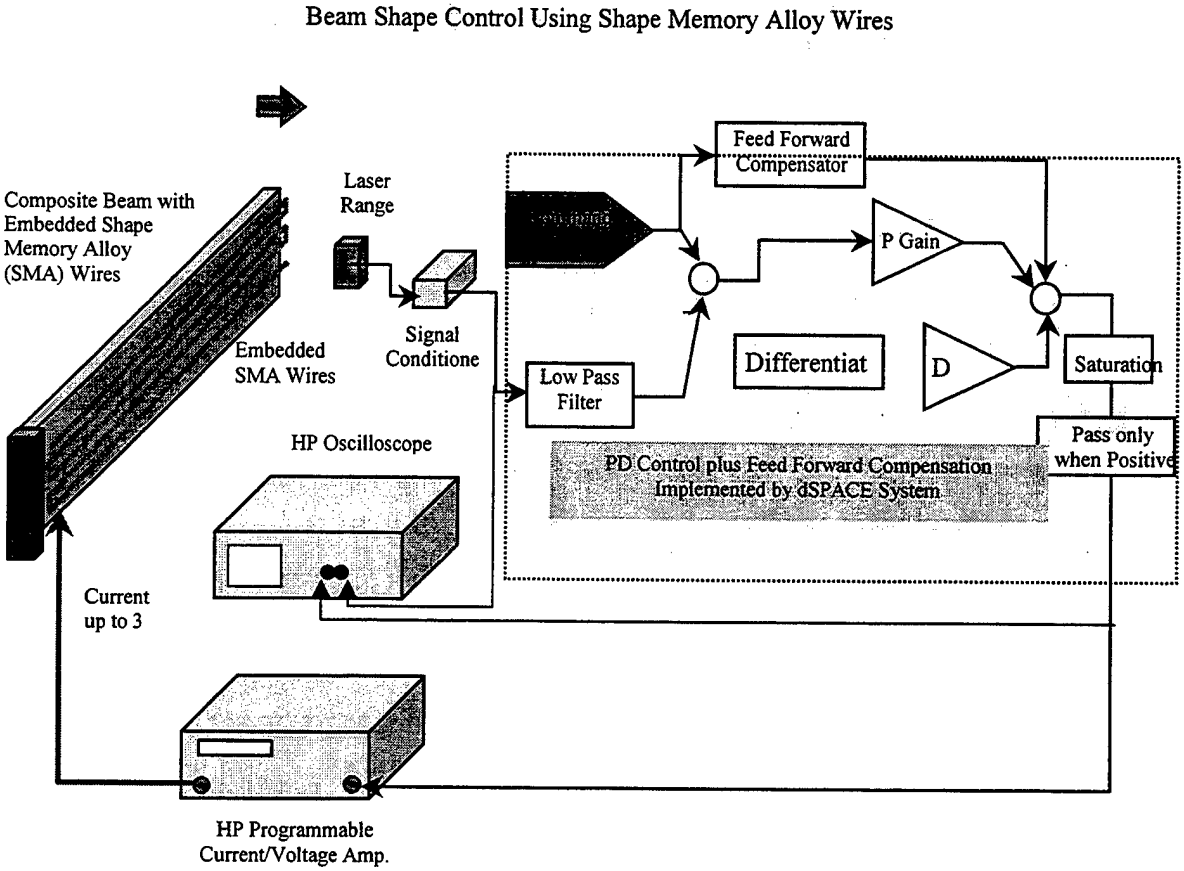

Figure 12. Shape memory beam experiment block diagram

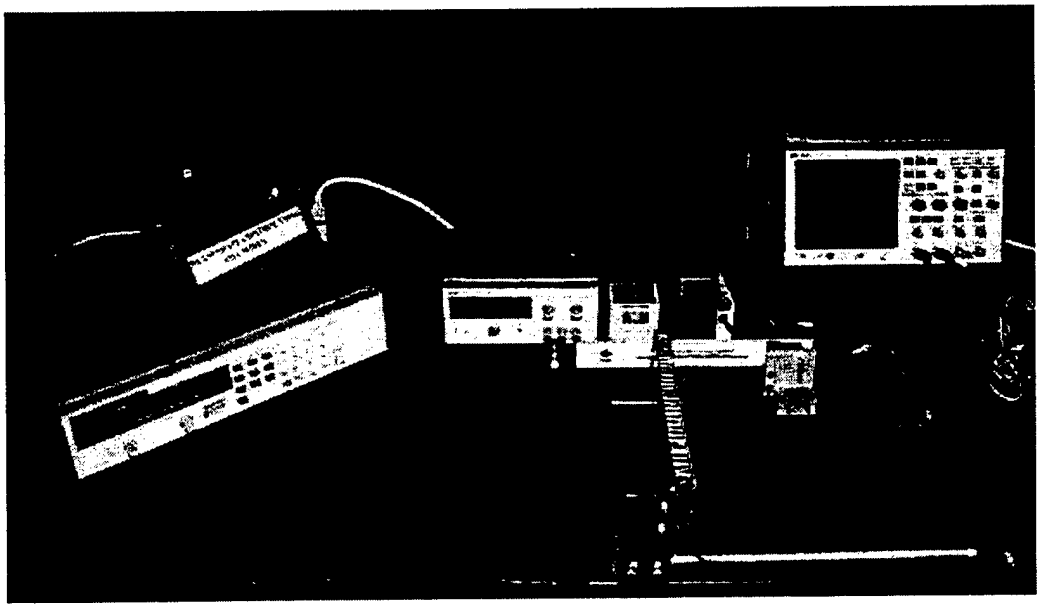

Figure 13. Shape memory alloy beam experiment

B. EQUIPMENT DESCRIPTION

1. Single Wire Test Stand

The single wire test stand as the name implies is a structure that provides the capability of experimenting with a single wire. The single wire test stand is shown in Figure 14. The shape memory wire was attached between two wire supports. One wire support was attached to a rod that is free to slide through linear bearings. The rod was attached to a biasing spring which pretensions the shape memory wire. As the shape memory wire was heated, it contracted, which placed tension on the spring.

2. Shape Memory Alloy Wire

The shape memory alloy wires used were a binary nickel-titanium (nominal austenite temperature of 70 °C) with a diameter of 0.381 mm. These wires were pre-

strained to 3% and heat treated to provide the shape memory effect. These wires are capable of being cycled millions of times over large strains (>3%), and at high stress levels (>350 MPa).

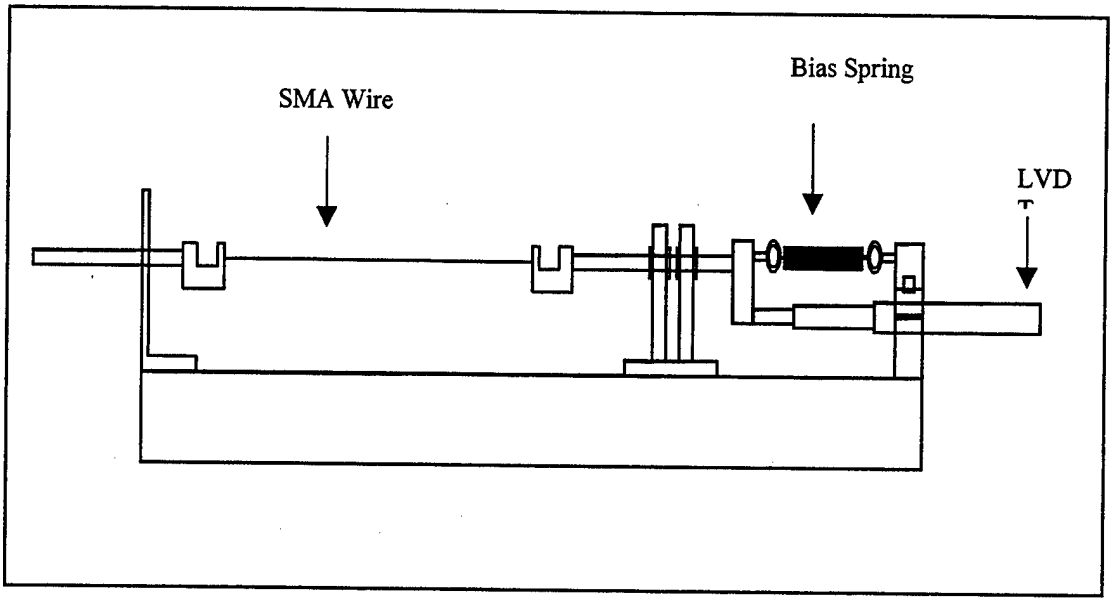

Figure 14. Single wire test stand

3. Shape Memory Alloy Composite Beam

Lockheed Martin provided NPS with two shape memory composite beams. The beams use shape memory wires to deform the structure. These wires are embedded within a low modulus elastomeric facesheet attached to honeycomb core. The opposing side of the beam consists of a high modulus glass epoxy bonded to honeycomb core. The elasticity of the beam provides the restoring force. Beam 1 was constructed of a 1.27 cm thick 5052 aluminum honeycomb core, with a 0.81 mm thick G-10 backbone, a 2.54 mm thick Conathane® urethane casting system UC-49 compliant facesheet, and two ultem 2300 termination blocks. There are sixteen 0.381 mm diameter, 30.48 cm, nickel-titanium shape memory wires (two seried sets of eight wires electrically wired in parallel) embedded in the compliant facesheet. The corresponding circuit resistance of the wires was 10.3 ohms. The overall dimensions of the beam are 30.48 cm long, 5.08 cm wide and 1.32 cm thick. Figure 15 is a top view diagram of the beam, and Figure 16 is a side

view of the beam. The shape memory composite beam was activated by supplying direct current ranging from 1.5 – 3.0 amps to the shape memory alloy wires. The exact amount of current depends on the desired response time and degree of actuation. Current in excess of 3 amps or extended hold times at maximum deflection can result in degradation of the urethane facesheet.

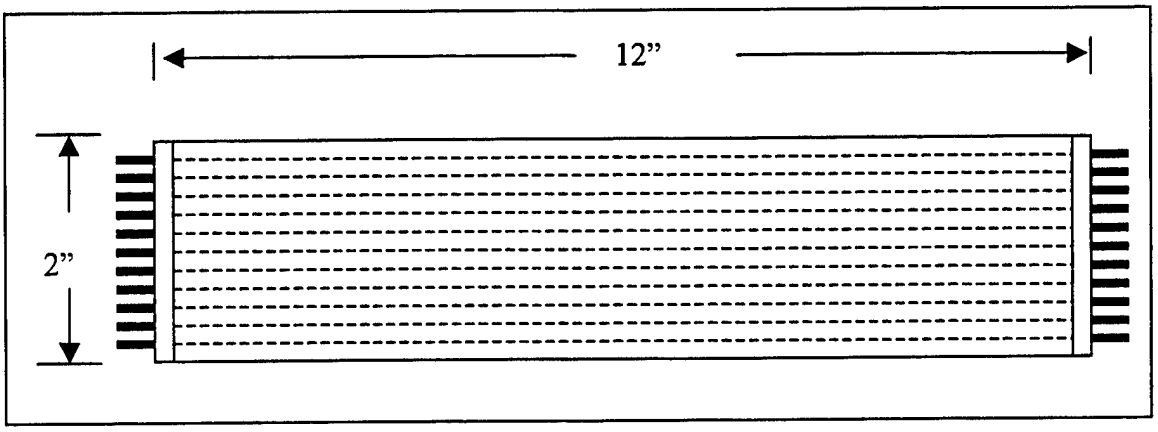

Figure 15. Shape memory composite beam (top view)

Shape memory composite beam 2 construction was identical to beam 1 with the exception of the aluminum honeycomb core and the thickness of the G-10 backbone. The core of beam 2 is 1.59 cm thick aluminum F80 flexcore®, and the G-10 backbone is 1.14 mm thick vice the 0.81 mm backbone in beam 1. Beam 2 contains the same number of shape memory wires, and has the same electrical circuit resistance of 10.3 ohms. Figure 17 is an actual picture of the shape memory composite beam and some shape memory wires.

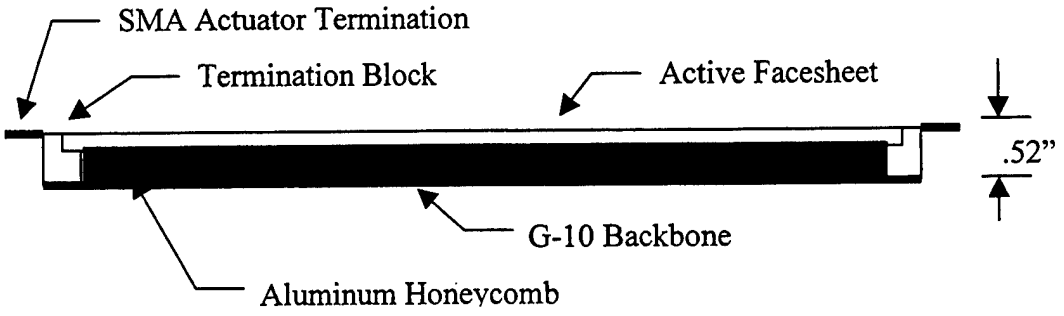

Figure 16. Shape memory composite beam (side view)

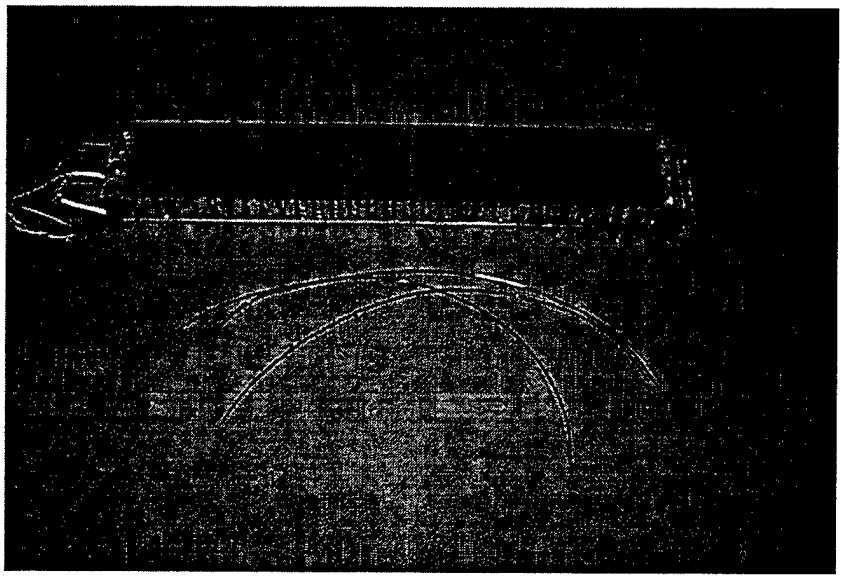

Figure 17. Shape memory composite beam

4. Hewlett Packard Programmable Power Supply

The HP programmable power supply model 6542A supplied current to the shape memory wire. The power supply had a range of 0 – 20 volts, or 0 – 10 amps. It can be programmed to operate in either a voltage control mode or a current control mode. In the voltage control mode, the power output voltage is proportional to an input voltage. The input voltage range is 0 – 5 volts', therefore, a 1 volt input to the power supply corresponds to 4 volt output from the power supply. The output voltage from dSpace is the input voltage to the power supply.

For the current control mode, the power supply output current is proportional to an input voltage. Again, the input voltage range is 0 – 5 volts, therefore a 1 volt input would correspond to a 2 amp output from the power supply for a constant load resistance. The power supply was operated in the voltage control mode for both the single wire and composite beam experiment.

5. Linear Variable Differential Transformer (LVDT)

An LVDT manufactured by Lucas Controls Systems was used to measure the wire displacement in the single wire experiment. The LVDT requires a ±15 VDC power supply for operation. The output range of the LVDT is –15 to +15 VDC, which is proportional to the position of the wire.

6. NAIS Laser Analog Sensor (LM100)

A NAIS laser analog sensor (model LM100) was used in the shape memory beam experiment to measure beam tip displacement. The measurable range of the laser sensor is 80 – 180 mm, and has a output voltage range from –5 to +5 VDC.

IV. SINGLE WIRE CONTROL SYSTEM DESIGN AND IMPLEMENTATION

The intent of a single wire experiment is to gain an understanding of control of shape memory materials prior to attempting to implement control of the more complex shape memory composite beam. A single nickel titanium wire (28 cm in length, and 0.381 mm in diameter) was attached to the single wire test stand. One end of the wire was attached to the fixed end of the stand, and the other end of the wire was attached to the biasing spring by a threaded rod, which is free to slide through linear bearings. Applying a current to the SMA wire causes it to actuate. The rate at which the SMA wire actuates depends on the magnitude of the applied current. Nickel titanium SMA wires require 1.5 to 3.0 amps to actuate. An actuation current less than 1.5 amps will actuate the wire, however the actuation is very slow.

An empirical approach was used to design a position control system for the SMA wire. Figure 18 depicts the direction of movement of the SMA wire; Δx is the desired change in length of the SMA wire. The control scheme accepts a Δx as input, and current applied to the SMA wire actuates it to the given length and maintains that length.

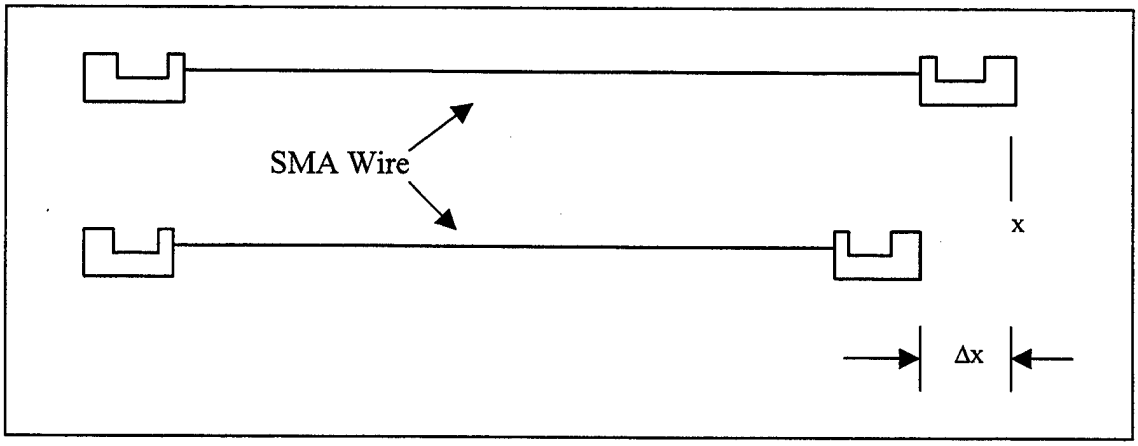

Figure 18. SMA wire movement

Prior to designing a position control system for the SMA wire, it was necessary to actuate the wire with different values of current to determine a reasonable maximum

actuation rate and the maximum amount of travel possible with the single wire test stand. The HP programmable power supply provided the current to the SMA wire, and an additional HP DC power supply was used to provide a control voltage to the programmable power supply. The SMA wire was actuated several times using an actuation current between 1.5 – 3.0 amps. It was found that the maximum displacement (Δx) is approximately 13 cm, and a reasonable maximum actuation current is 1.5 amps. The SMA wire is capable of displacement of up to 8% of its original length, and the length of SMA wire used in this experiment is 28 cm. Therefore the theoretical maximum displacement is 2.24 cm. The single wire test stand could be adjusted to allow for the maximum theoretical displacement, but 1.3 cm was sufficient for this application. An actuation current greater than 1.5 amps causes the SMA wire to contract at a speed that is to great to be easily controlled. Increasing the actuation current results in an overshoot of the desired position. Overshoot significantly increases the settling time for the SMA wire. This is because heating of the SMA wire causes contraction, while expansion, or returning to its original shape, is due to cooling of the SMA wire. The cooling rate of the SMA wire is a function of the surrounding temperature and the amount of airflow across the SMA wire. The experiment is not designed to compensate for the surrounding temperature or the airflow across the SMA wire, therefore to minimize settling time it is best to slow the rate to avoid overshoot.

A. PROPORTIONAL-INTEGRAL-DERIVATIVE CONTROL

The empirical approach to design was chosen due to the difficulty of modeling SMA materials. Therefore, the first attempt for position control was to design a proportional-integral-derivative (PID) controller and then tune the parameters in order to obtain a stable system. The output of the PID controller is given by equation 1.

$$u = k_p e + k_i \int_0^t e dt + k_d \frac{de}{dt} \tag{1}$$

Where u is the output of the controller, e is the position error, k_p is the proportional gain (P-gain), k_I is the integral gain (I-gain), and k_d is the derivative gain (D-gain). A block diagram of the PID controller is shown in Figure 19.

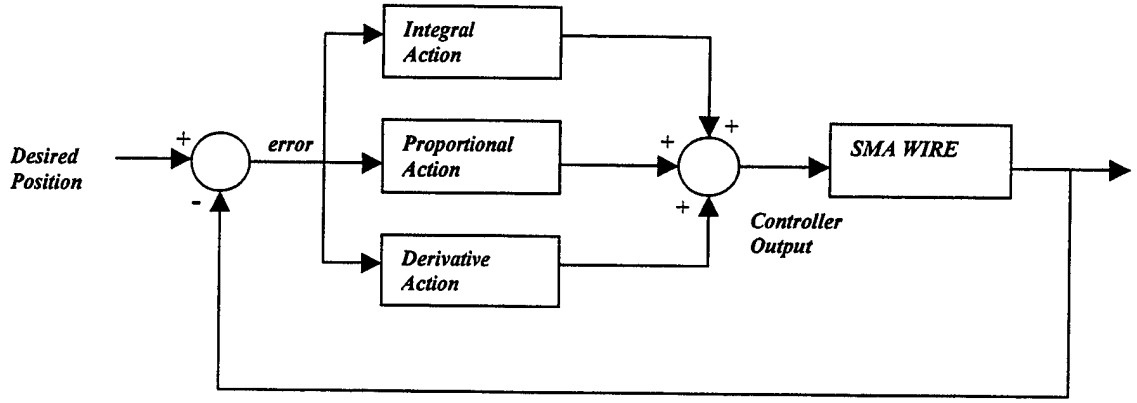

Figure 19. Block diagram of PID controller

The control system was designed using MATLAB/Simulink and implemented using the dSpace real time control system. The dSpace real time control system allows the user to change the control parameters without reloading the program after each change.

As a starting point for the PID controller, the proportional gain was set to 15, the derivative gain to 10 and the integral gain to 10. With an ordered displacement of 3mm and a maximum actuation current of 1.5 amps, there was a delay in response, and significant overshoot. The PID gains were then adjusted in order to reduce the overshoot. The results are shown in Figures 20-23.

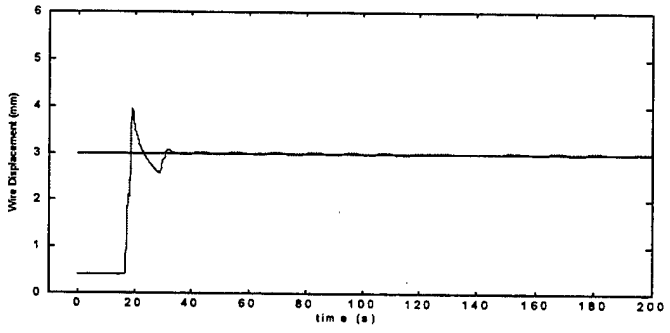

Figure 20. P-gain = 15, D-gain = 10, I-gain = 10

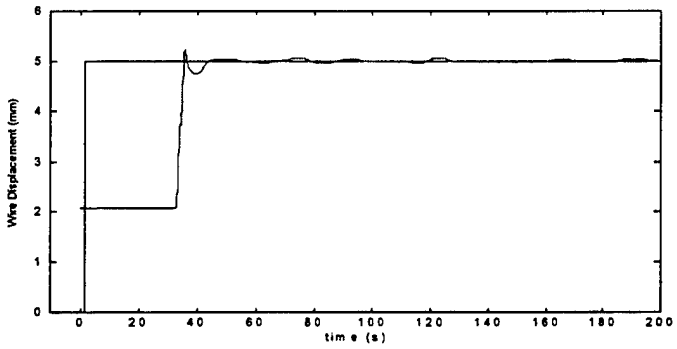

Figure 21. P-gain = 5, D-gain = 2, I-gain = 2

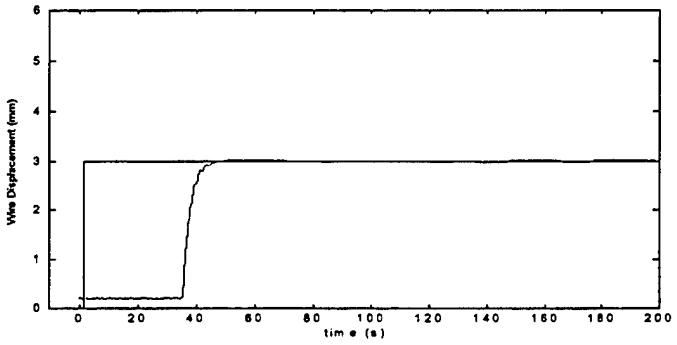

Figure 22. P-gain = 5, D-gain = 2, I-gain = 1.5

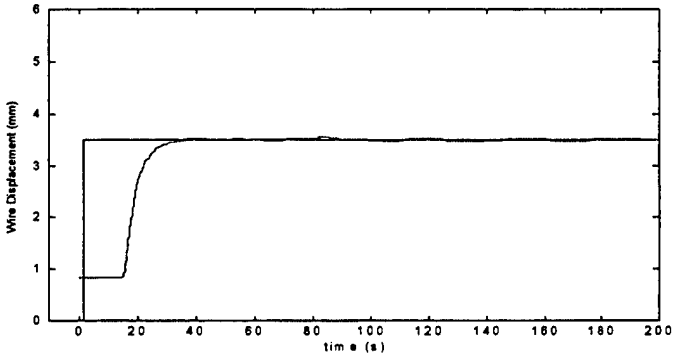

Figure 23. P-gain = 5, D-gain = 2, I-gain = 1.1

It can be seen that PID control provides very accurate position control, with very fast settling times. The problem is that the integral term sums the history of the position error. This is a problem because the wire can only be controlled in one direction, and if the LVDT is calibrated to a zero reference point and then the wire is actuated, because of

the temperature hysteresis, the wire length will not return to its original length after actuation. For example, if the starting point is zero, initially the position error is zero. If a displacement of 3mm is ordered, the wire is actuated, and after achieving the ordered position, a position of zero is ordered. The wire will expand but will not go back to zero. It will settle on some point greater than zero. This results in a negative position error, which the integral term then begins to sum, this can result in a very large negative number depending on the length of time between actuations. Then if a position is ordered which is greater than the actual position, there will be a delay in response until the integral term has a sum that is greater than zero. Therefore the integral term was set to zero and an attempt was made to design an accurate control system using a PD controller.

B. PROPORTIONAL-DERIVATIVE CONTROL

The first attempt at using PD control is shown in Figure 24. The delay in response has been eliminated, but there is a very large position error (approximately 0.6mm).

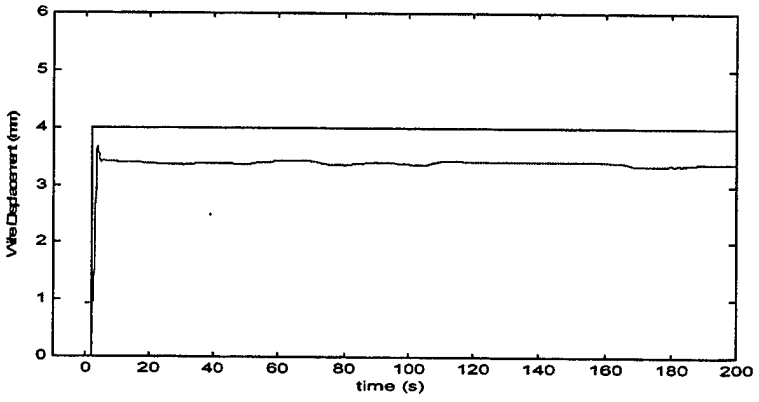

Figure 24. P-gain = 5, D-gain = 2

This is because as the SMA wire approached the desired position, the actuation current went to zero. Without actuation current, the SMA wire cools immediately, and begins to expand. In the PID control case, the integral term would compensate for this heat loss. Since the integral term has been set to zero, another method must be used to compensate

for the heat loss. A bias voltage was added that would compensate for this heat loss, but first, the value of a bias voltage had to be determined. The resistance of is the SMA wire is found using equation 1.

$$R = \rho \times \frac{l}{A} \tag{2}$$

where ρ is the resistivity, l is the length of the wire, and A is the cross sectional area of the wire. In the 100% martensite phase, the SMA wire has a resistivity of approximately 80 μΩ cm, and in the 100% austenite phase the resistivity is approximately 100 μΩ cm. The diameter of the SMA wire used in this experiment is 0.381 mm, which has a cross sectional area of 0.00115 cm^2. The 100% martensite resistance is 1.96 Ω, and the 100% austenite resistance is 2.46 Ω. When the SMA wire is in the 100% martensite phase, the bias voltage results in a current of 0.765 amps through the wire, but at the 100% austenite phase, the bias current is only 0.609 amps. The bias voltage should provide a current that is less than the minimum actuation current (1.5 amps). Several experiments were conducted for a 3mm displacement and for various values of bias voltage. A bias voltage range of 0.01 – 0.04 vdc was chosen for these experiments. This range was chosen because the actuation current range for the wire was 1.5 – 3.0 amps, and this experiment was limited to a maximum current of 2.0 amps due to the voltage limitations of the HP programmable power supply. The dSpace real time control system multiplies all input voltages by 0.1 and all output voltages by 10, therefore a bias voltage range of 0.01 – 0.04 vdc added to the output corresponds to a range of 0.4 – 1.6 vdc actually applied to the wire (Table 2).

Bias Voltage	**Actual Voltage**
0.01	0.4
0.02	0.8
0.03	1.2
0.04	1.6

Table 2. Bias voltage to actual voltage relationship

The output of the PD controller with feed-forward compensation (bias voltage) is given by equation 3.

$$u = bias + k_p e + k_d \frac{de}{dt} \tag{3}$$

Where bias is the feedforward compensator. This is shown in block diagram form in Figure 25.

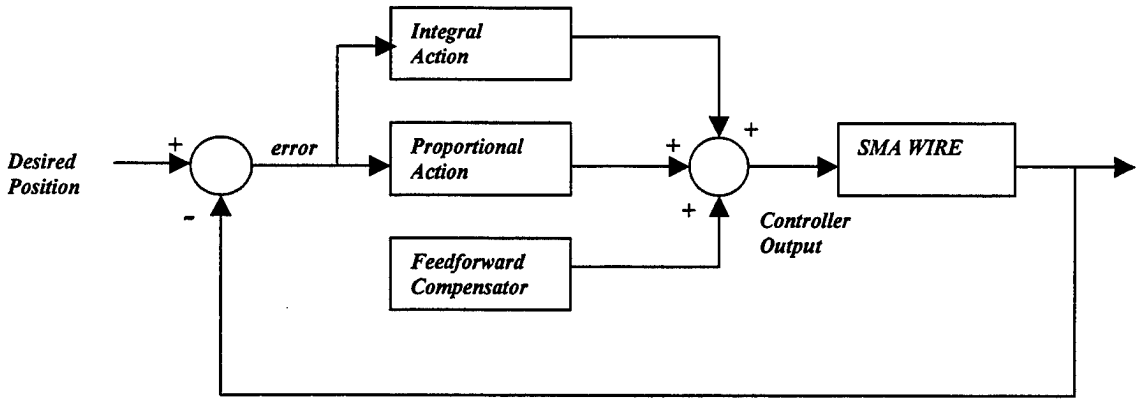

Figure 25. Block diagram of PD controller with feedforward compensation

The results of these experiments are shown in Figures 26 - 29. As the bias voltage is increased the position error decreases, but overshoot occurs.

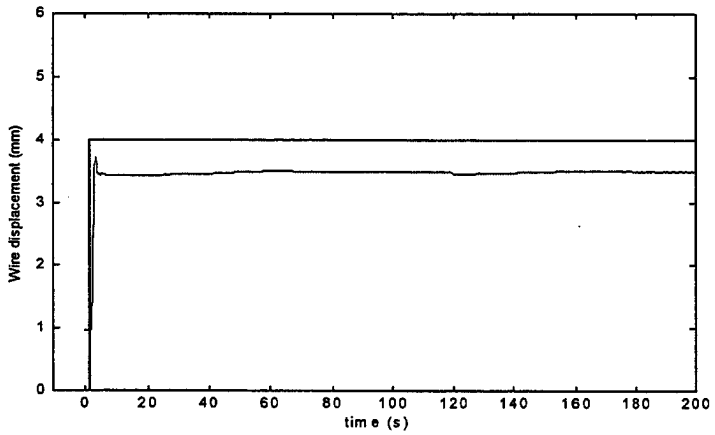

Figure 26. P-gain = 5, D-gain = 2, bias voltage = 0.01

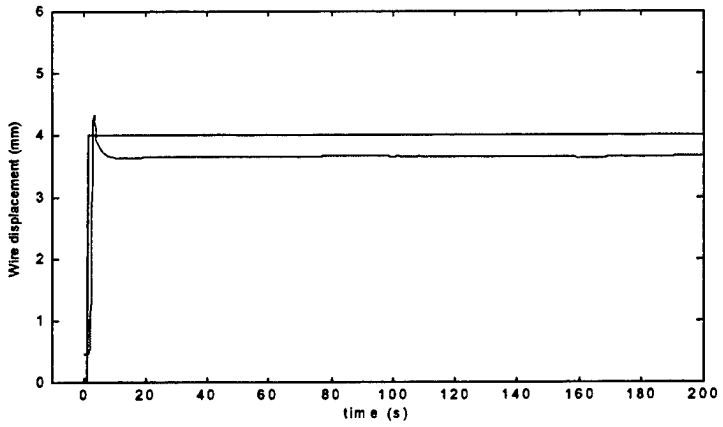

Figure 27. P-gain = 5, D-gain = 2, bias voltage = 0.02

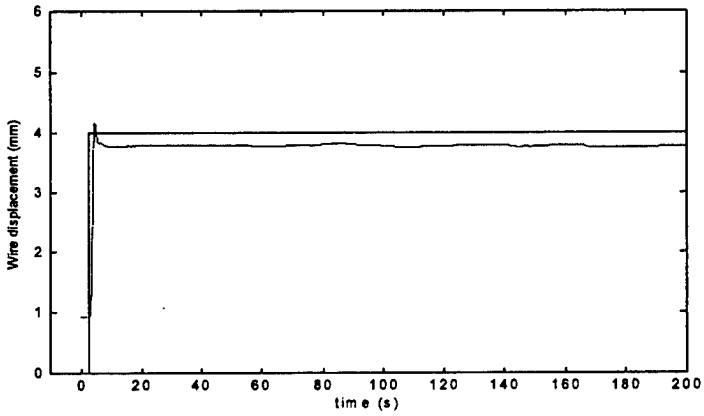

Figure 28. P-gain = 5, D-gain = 2, bias voltage = 0.03

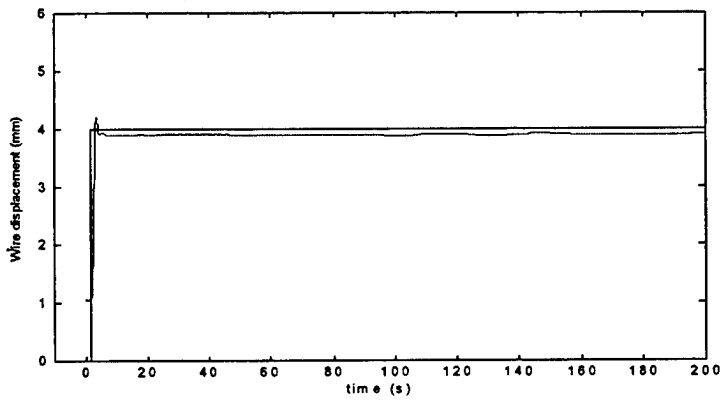

Figure 29. P-gain = 5, D-gain = 2, bias voltage = 0.04

A case with a bias voltage of 0.05 vdc was tried, but the wire settled on a position greater than the ordered position. Finally, a case with a bias voltage of 0.045 vdc was tried, and this provided a very small (0.02mm) position error (Figure 30), but the overshoot still occured.

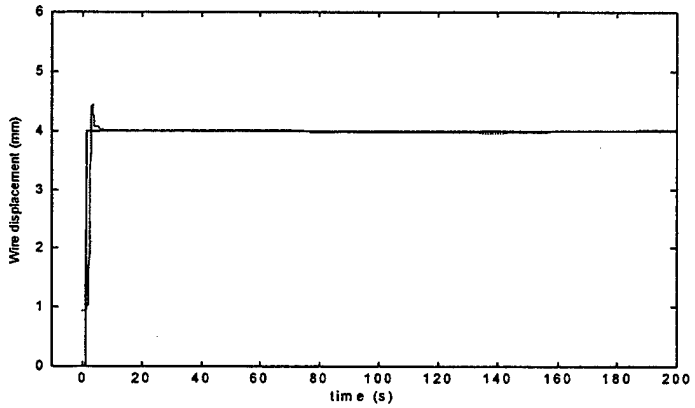

Figure 30. P-gain = 5, D-gain = 2, bias voltage = 0.045

A bias voltage of 0.045 vdc provides a very accurate position control for a 3mm displacement, but it must be determined if this bias voltage is sufficient for other displacements. Two experiments were conducted, one for a displacement of 2.5mm and one for a displacement of 4.5mm, both with a bias voltage of 0.045 vdc. The shape memory material changes resistance as phase change occurs. Larger displacements require a greater amount of phase change, and conversely smaller displacements require smaller amounts of phase change. Therefore, it is expected that for a 2.5mm displacement, a bias voltage of 0.045 vdc will be too much. This turned out to be the case, as is shown in Figure 31. The wire displacement exceeded the ordered displacement. This would suggest that a displacement of 4.5mm would require a bias voltage greater than 0.045 vdc, but as shown in Figure 32, this was not the case. This is most likely due the increase in the wire strain for the larger displacement.

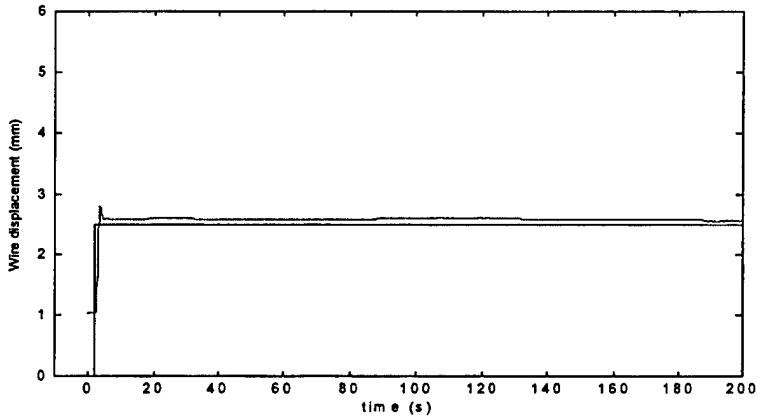

Figure 31. 2.5mm displacement with 0.045 vdc bias voltage

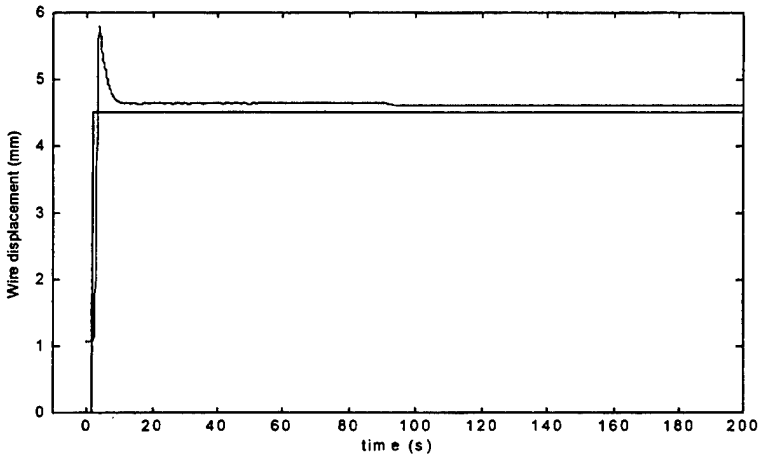

Figure 32. 3.5mm displacement with 0.045 vdc bias voltage

A very accurate position control has been achieved for a 3mm displacement, but it is desirable to eliminate the overshoot. The proportional and derivative gains were adjusted in order to accomplish this. Figures 33 - 35 show the results with various proportional and derivative gains.

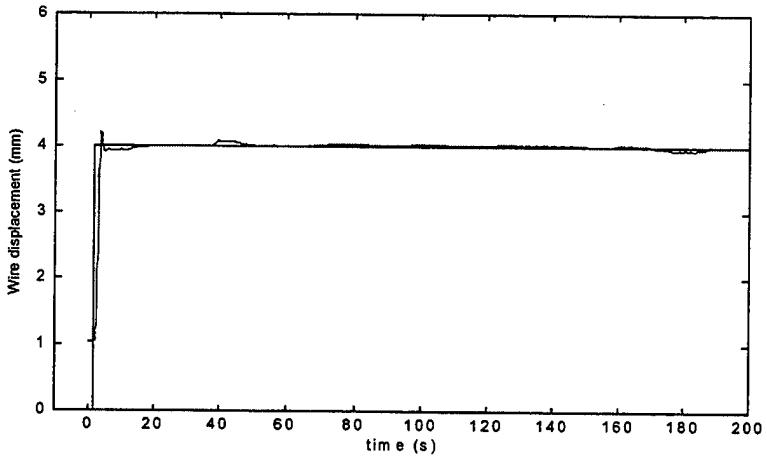

Figure 33. P-gain = 4, D-gain = 2

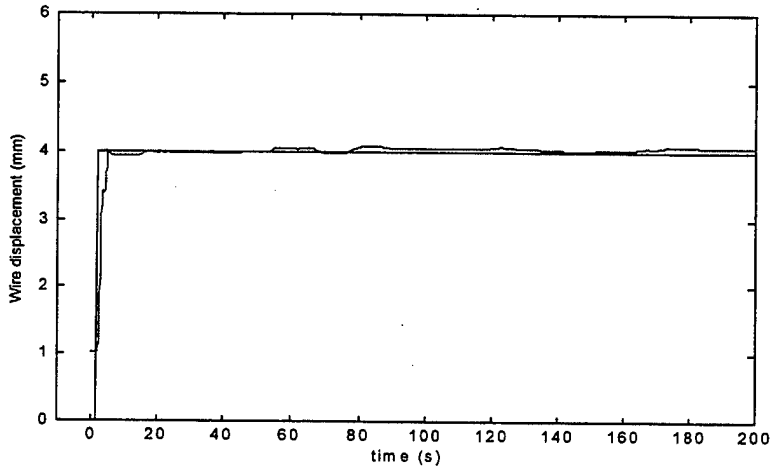

Figure 34. P-gain = 3, D-gain = 2

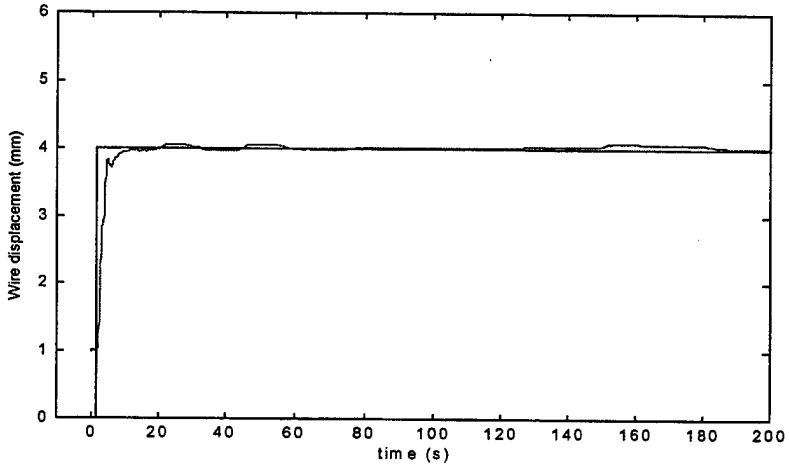

Figure 35. P-gain = 2.5, D-gain = 2.5

As seen in Figure 35, a proportional gain of 2.5 and a derivative gain of 2.5 provided a very accurate position control with no overshoot, for a 3mm displacement. Figure 36 shows the MATLAB/Simulink representation of the control system used in this experiment.

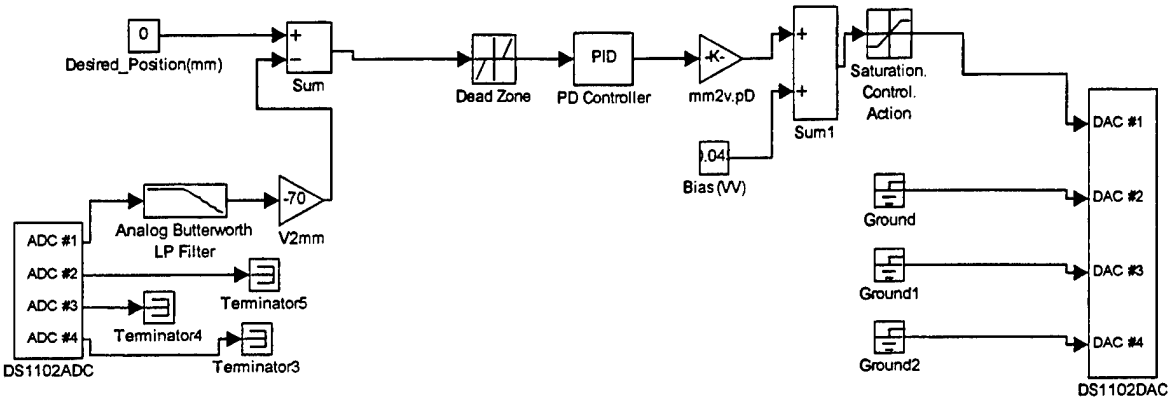

Figure 36. MATLAB/Simulink Representation of the PD Control Feedforward Compensator

Additional components of the PD controller not mentioned earlier are a low pass filter, which filters out high frequency components from the laser sensor, a dead zone function, which limits the position control accuracy to ± 0.01mm, and a saturation function, which limits the magnitude of the output voltage to 0.5 vdc. This corresponds to maximum voltage across the composite beam of 20 vdc, which is the HP programmable power supply's maximum rated output voltage. Also there are gains on the input and output which first converts the input voltage to a voltage proportional to the displacement in millimeters. The LVDT output is in volts per centimeter, and the control range is in millimeters, therefore the input is converted to millimeters and then converted back to centimeters on the output.

V. SHAPE MEMORY ALLOY COMPOSITE BEAM CONTROL SYSTEM DESIGN AND IMPLEMENTATION

The intent of the shape memory composite beam experiment is to demonstrate the ability to perform position control of the shape memory composite beam. The experimental setup was shown in Chapter III.

The first step in designing a control system would be to develop an analytical model. Due to the non-linearities of SMA's, developing an analytical model is difficult. Additionally, the mechanical properties of the facesheet and the G-10 backbone were not provided. Without these properties, modeling the SMA composite beam is impossible. Therefore an empirical approach was used to design a position control system for the SMA composite beam. Figure 37 shows a top view of the SMA composite beam. The end at point O is constrained and the end at point A (the beam tip) is free to move in the ±y direction. The SMA wires are embedded on the –y face. As current is applied to the SMA beam, the beam tip will displace in the –y direction, and when the current is removed, the beam tip will move in the y direction towards its starting position.

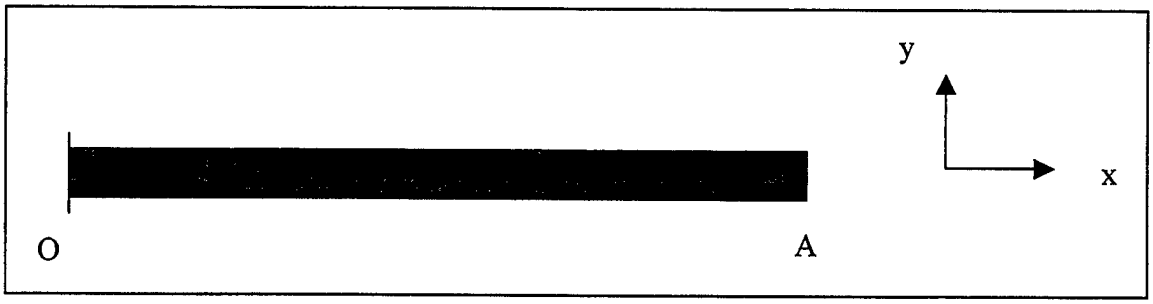

Figure 37. SMA composite beam (top view)

Prior to designing a position control system for the SMA beam, it was necessary to actuate the SMA beam with different values of current to determine a reasonable actuation rate and the maximum displacement of the beam tip. This was accomplished by using an additional HP DC power supply to provide a control voltage to the HP programmable power supply. The SMA beam was actuated several times using an actuation current between 1.5 – 2.0 amps. It was found that the maximum displacement

of the SMA beam tip was approximately 7mm, and a reasonable actuation current was 2.0 amps. To determine the theoretical maximum displacement of the beam tip, the mechanical properties of the SMA beam elements must be known. The mechanical properties of the aluminum honeycomb core are known, but the properties of the active facesheet and the G-10 backbone were not provided. Therefore, based on observations, it was determined that 7 mm was a reasonable maximum displacement. An actuation current of greater than 2.0 amps would have probably provided faster response time, but the HP programmable power supply was limited to an output voltage of 20 volts. The equivalent resistance of the SMA wires in the beam was 10.3 Ω, so the maximum current possible was 1.94 amps.

A. PROPORTIONAL-INTEGRAL-DERIVATIVE CONTROL

The empirical approach to design was chosen due to the difficulty of modeling SMA materials; therefore, the first attempt for position control was to design a proportional-integral-derivative (PID) controller and then tune the gains in order to obtain a stable system. The output from a PID controller is given by equation 1.

$$u = k_p e + k_i \int_0^t e dt + k_d \frac{de}{dt} \tag{4}$$

Where u is the output of the controller, e is the position error, k_p is the proportional gain (P-gain), k_I is the integral gain (I-gain), and k_d is the derivative gain (D-gain). The PID controller is shown in block diagram from in Figure 38.

The control system was designed using MATLAB/Simulink and implemented using the dSpace real time control system. The dSpace real time control system allows the user to change the control parameters without reloading the program after each change.

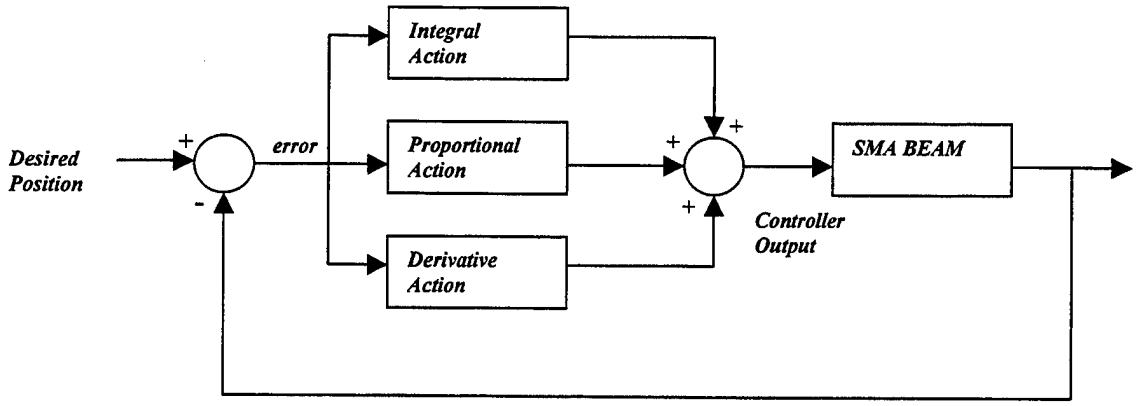

Figure 38. PID controller block diagram

As a starting point, the P-gain was set to 35, the D-gain set to 20 and the I-gain was set to 20. A desired position which would result in a displacement of 3.5 mm was ordered, and as seen in Figure 39, there was a delay in response to the position error, and the beam tip traveled past the desired position. The beam tip oscillated about the desired position before settling at the desired position. As with the single wire experiment, the delay in response was due to the integral term summing the history of the position error.

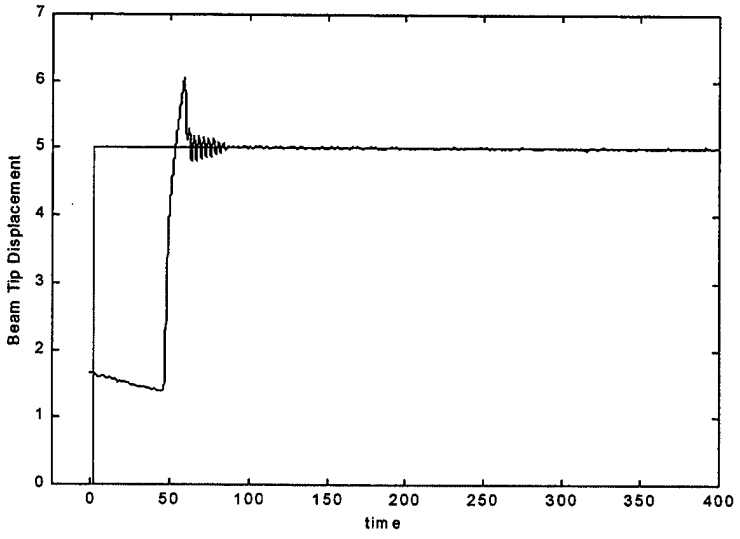

Figure 39. P-gain = 35, D-gain = 20, I-gain 20

The I-gain was reduced to 5 in an attempt to eliminate the overshoot. This resulted in a small reduction in the overshoot (figure 40) for the 3.5mm displacement.

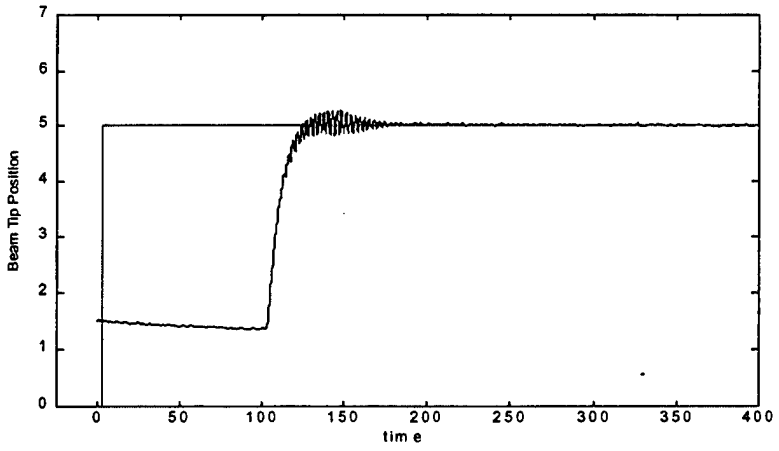

Figure 40. P-gain = 35, D-gain = 20, I-gain 5

Although the PID control provides very accurate position control and fast settling time, the delay in response due to the integral term, and the overshoot, are problems that must be corrected in order to achieve a responsive system. Additionally, if the beam has not been actuated for a long period of time (24 hours or so, the beam is cold), its response will be very slow until it heats up. If the experiment using a PID control is conducted while the beam is cold, the system goes unstable and the beam tip will continue past the desired position until the experiment is shut down. The data shown in figures 28 and 29 were taken after the beam had been actuated at least once to allow it to heat up. The I-gain was set to zero to try and eliminate the overshoot and the delay in response This resulted in a response with no overshoot, but with a large position error (0.77mm). Also there are oscillations in the beam tip as it approaches the desired position (Figure 41).

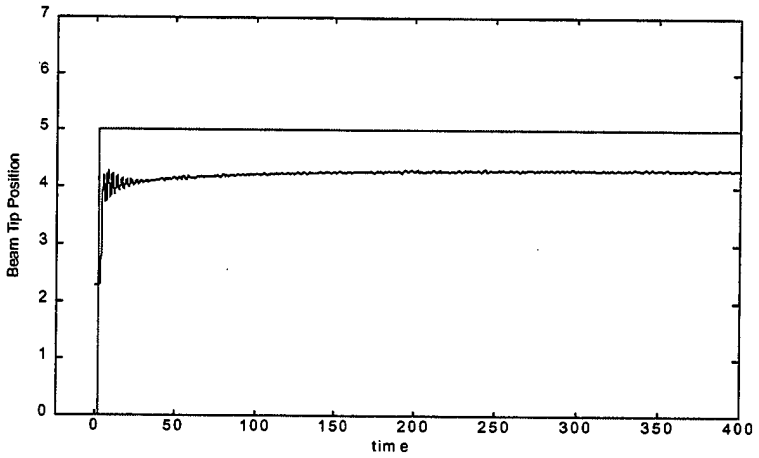

Figure 41. P-gain = 35, D-gain = 20, I-gain 0

B. PROPORTIONAL-DERIVATIVE CONTROLLER

The output of the PD controller is given by equation 2, and is the same as equation 1 without the integral term.

$$u = k_p e + k_d \frac{de}{dt} \tag{5}$$

Now that a PD controller is being used, the next step was to eliminate the beam tip oscillations and reduce the position error. The proportional gain was reduced to 20 and the experiment was conducted again for a displacement of 3.5mm. The results are shown in figure 42. The beam tip oscillations decreased significantly, but were not eliminated. Additionally, the position error increased to 1.22mm.

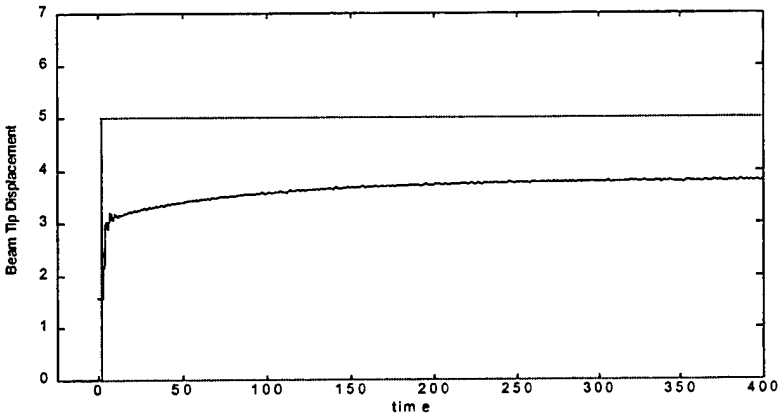

Figure 42. P-gain = 20, D-gain = 20

The next step was to eliminate the position error without introducing oscillations into the beam. The position error was due to heat loss from the SMA material. The control system was supplying current to the beam to actuate it to the desired position, but the SMA material was dissipating heat through I^2R losses. To compensate for this heat loss, a bias voltage was added (feedforward compensator) to the PD controller. The magnitude of this bias voltage had to be determined. To do this, several experiments were conducted for a 3.5mm displacement, and for various values of bias voltage. A bias voltage range of 0.1 – 0.3 vdc was chosen for this these experiments. This range was chosen because the actuation current range for the composite beam was 1.5 – 3.0 amps, and this experiment was limited to a maximum current of 2.0 amps due to the limitations of the HP programmable power supply. The dSpace real time control system multiplies all input voltages by 0.1 and all output voltages by 10, therefore, a range of 0.1 – 0.3 vdc added to the output corresponds to a range of 4 – 12 vdc actually applied to the composite beam (Table 3).

Bias Voltage Setting	Actual Voltage
0.10 V	4 V
0.15 V	6 V
0.20 V	8 V
0.25 V	10 V
0.30 V	12 V

Table 3. Bias voltage to actual voltage relationship

The results of the experiments with various bias voltages, and the proportional and derivative gains set to 20 and a 3.5mm displacement are shown in Figures 43 - 46.

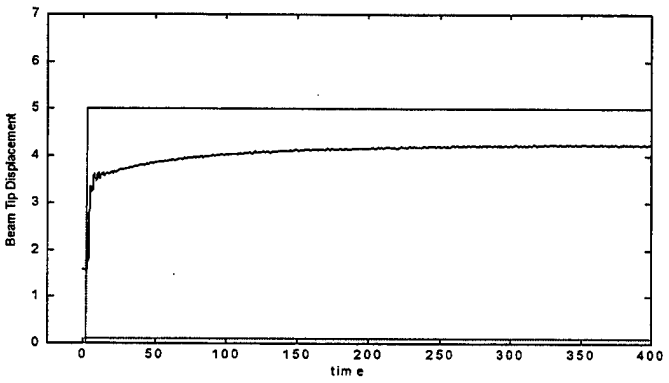

Figure 43. Bias Voltage = 0.1

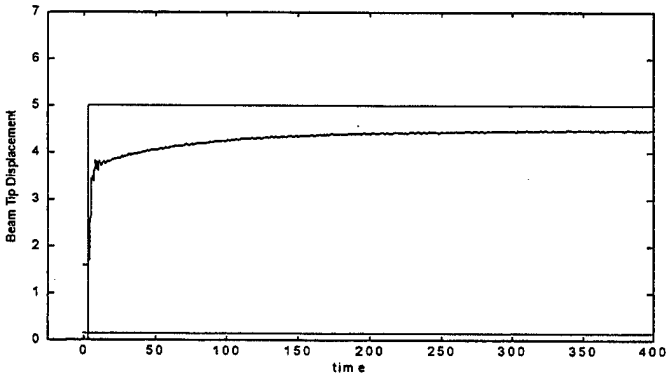

Figure 44. Bias Voltage = 0.15

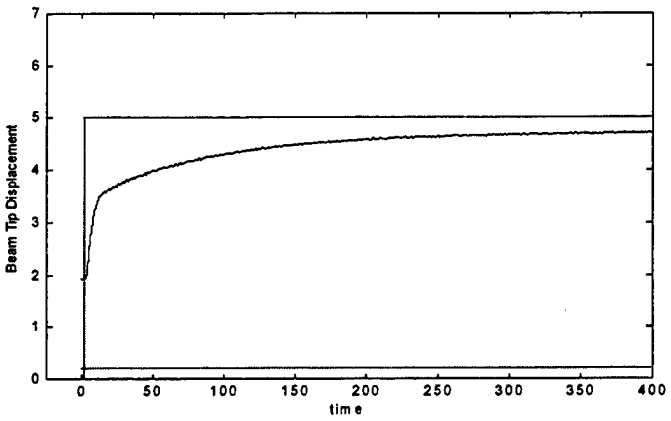

Figure 45. Bias Voltage = 0.2

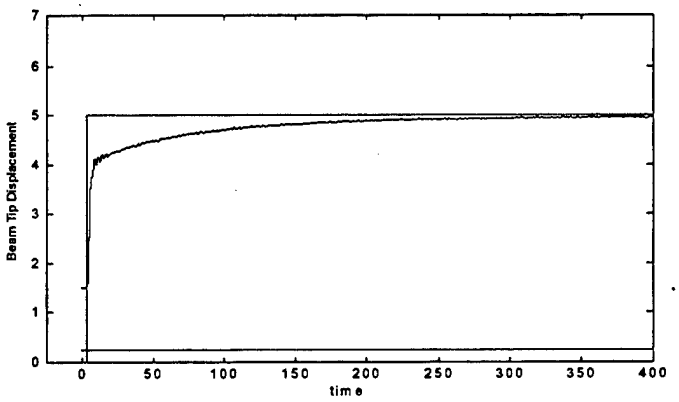

Figure 46. Bias Voltage = 0.25

A bias voltage of 0.3 vdc was tried, but it resulted in the beam tip position settling past the desired position; therefore, it can be seen that a bias voltage of 0.25 vdc provides the most accurate position control. Finally, experiments were conducted for a 4.5mm and 2.5mm displacement to determine if this bias voltage worked for other displacements. With the proportional and derivative gains still set to 20, a displacement of 4.5 mm was ordered, and the position error increased slightly from 0.03mm in the 3.5mm displacement case to 0.07mm (Figure 47).

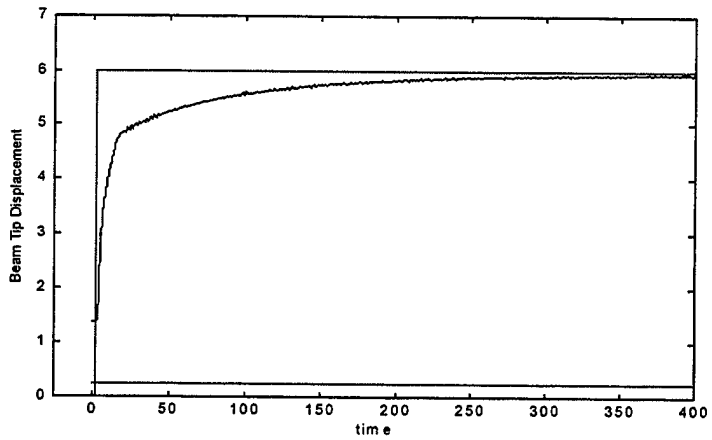

Figure 47. 4.5mm displacement with 0.25 vdc bias voltage

Again, with the proportional and derivative gains set to 20, a displacement of 2.5mm was ordered, and the beam tip position settled on a position greater than the desired position (Figure 48). This shows that for different displacements, different values of bias voltages are required to obtain the minimum position error. This is caused by the change in resistance of the shape memory material as it changes phase from martensite to austenite. Larger displacements result in a greater SMA wire resistance. As the resistance increases, a greater bias voltage is required to provide the required bias current.

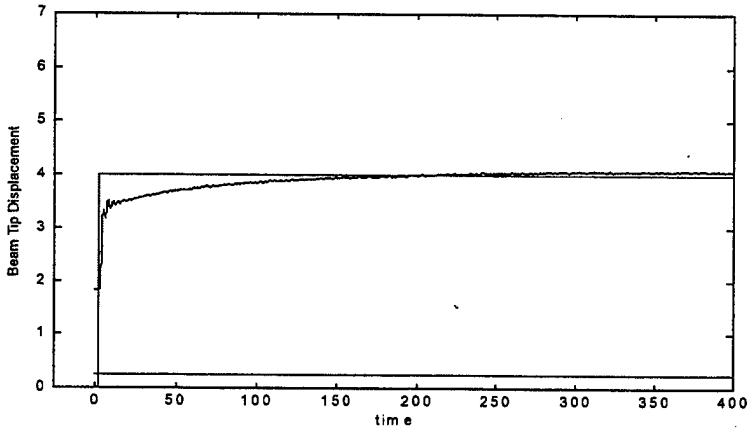

Figure 48. 2.5mm displacement with 0.25 vdc bias voltage

The output of the PD controller with feedforward compensation is given by equation 6.

$$u = bias + k_p e + k_d \frac{de}{dt} \tag{6}$$

Where the bias is the feed-forward compensation. The block diagram form is shown in Figure 49.

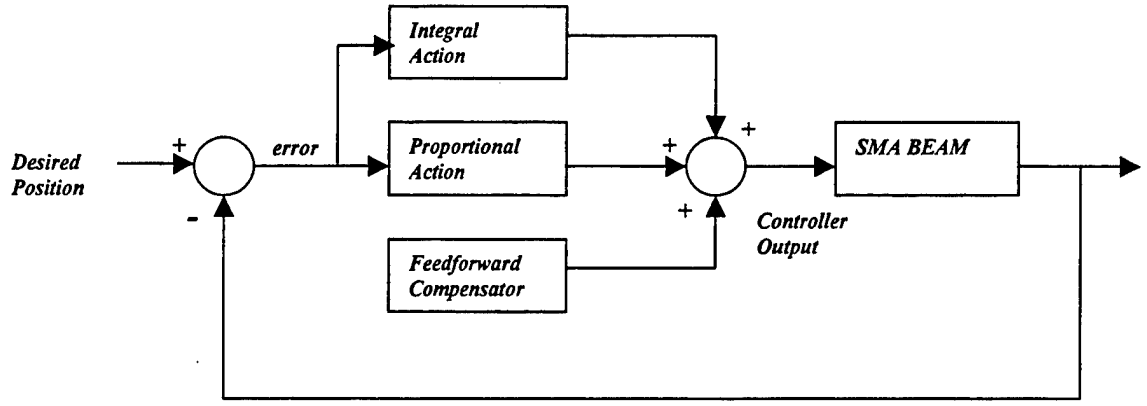

Figure 49. Block diagram of PD controller with feed-forward compensation

At this point an accurate position control using a PD controller has been developed for a displacement of approximately 3.5mm, but the transition from the starting point to the desired position is not smooth. There are still small oscillations in the beam tip as it approaches the desired position. This is due to the rate of actuation and the stiffness of the beam. Up to this point an actuation current of 2.0 amps has been used. This is the maximum current available from the HP programmable power supply. The programmable power supply was rated for an output voltage of 20 vdc, and the resistance of the SMA wires in the composite beam was 10.3 ohms. In an attempt to eliminate these oscillations, the actuation current was limited to 1.5 amps (the minimum required to actuate the beam). This resulted in a very smooth transition to the desired position (Figure 50).

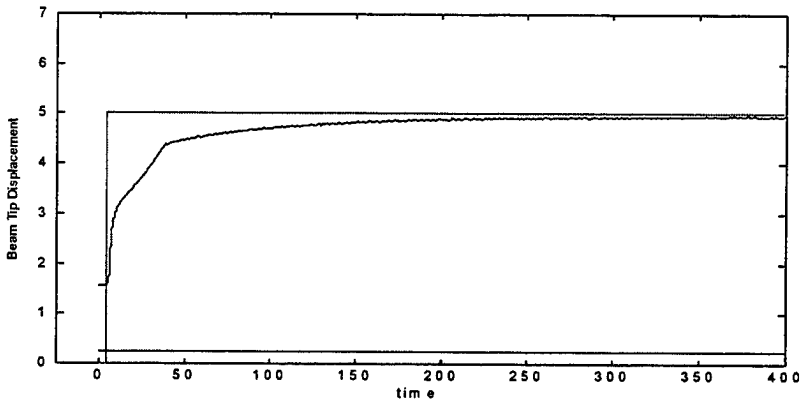

Figure 50. 3.5mm displacement with 1.5 amp actuation current

Although the position error has been reduced and the beam tip oscillation has been eliminated, the settling time is very large (approximately 400 seconds). Several attempts were made to adjust the proportional and derivative gains in order to reduce the settling time. Although small improvements were noted (Figures 51 and 52), these attempts were unsuccessful.

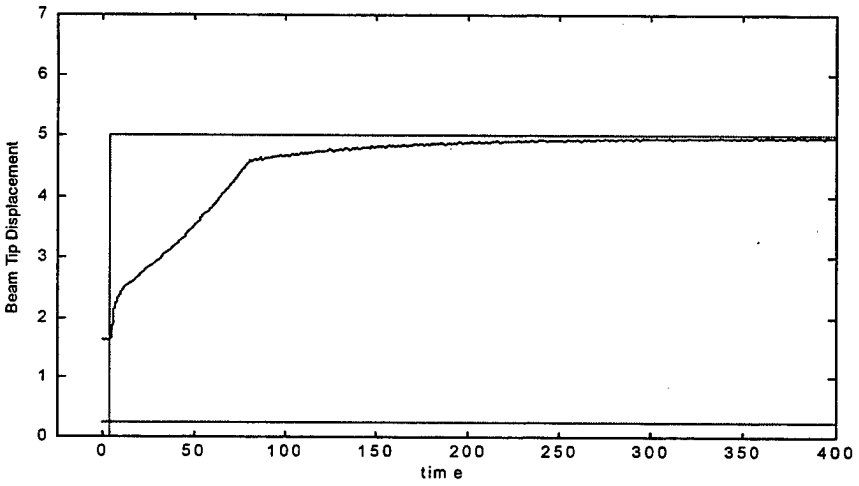

Figure 51. P-gain = 30, D-gain =20

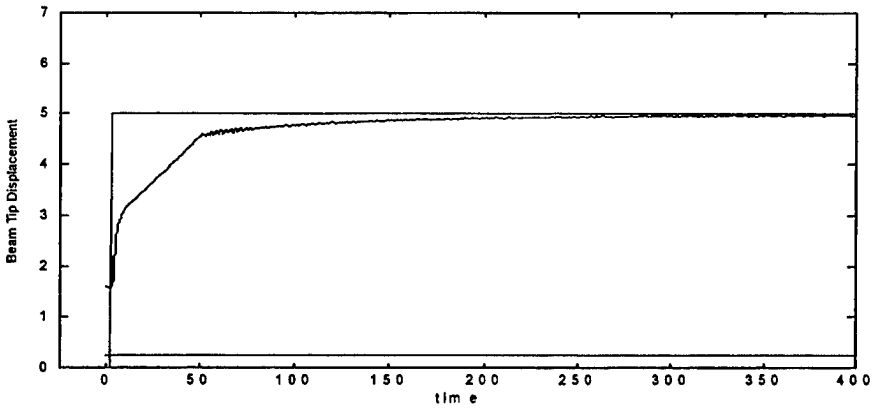

Figure 52. P-gain = 30, D-gain = 30

The MATLAB/Simulink representation of the PD controller with feed-forward compensator is shown in Figure 53.

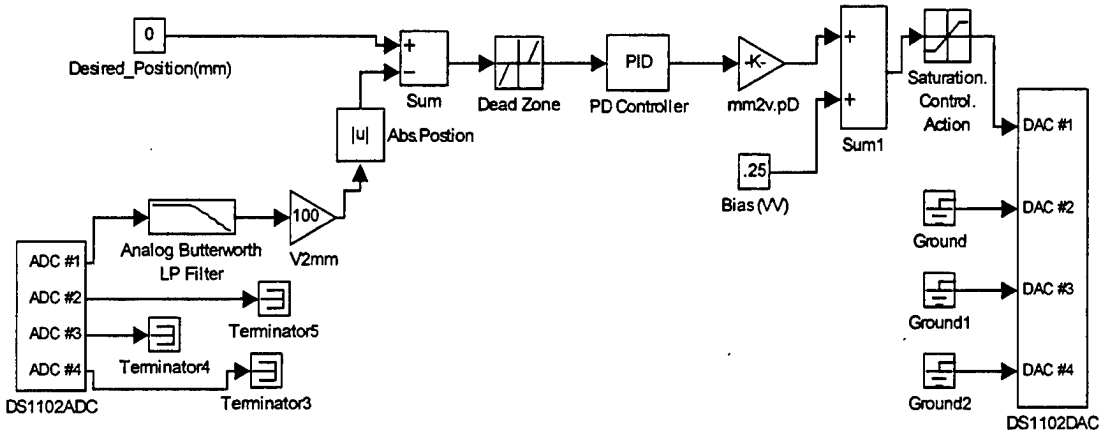

Figure 53. MATLAB/Simlink representation of the PD control with feedforward compensator

Additional components of the PD controller not mentioned earlier are a low pass filter, which filters out unwanted high frequency components from the laser sensor, a

dead zone function which limits the position control accuracy to ± 0.01mm, and a saturation function, which limits the magnitude of the output voltage to 0.5 vdc. This corresponds to maximum voltage across the composite beam of 20 vdc, which is the HP programmable power supply's maximum rated output voltage. Also there are gains on the input and output, which first converts the input voltage to a voltage proportional to the displacement in millimeters. The laser sensor output is in volts per centimeter, and the control range is in millimeters; therefore, the input is converted to millimeters and then converted back to centimeters on the output.

C. PROPORTIONAL-DERIVATIVE CONTROL WITH NON-LINEAR COMPENSATOR

The PD controller with a feed-forward compensator (bias voltage) provided accurate position control, but the settling time must be reduced in order to achieve a more responsive system. It has been shown that varying the proportional and derivative gains do not reduce the settling time. The actuation current could be increased to 2.0 amps, but this causes oscillations in the beam tip, therefore, a non-linear compensator was added to the PD controller. This non-linear compensator consisted of a hyperbolic tangent (tanh) function (Figure 54).

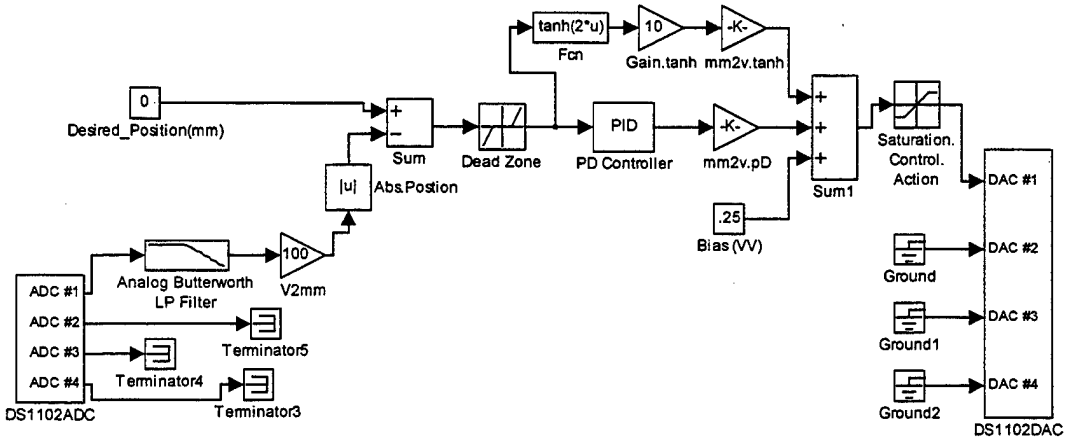

Figure 54. MATLAB/Simulink Representation of the PD Control with Non-Linear and Feedforward Compensator

Equation 4 is the input output relationship of the tanh function.

$$y = \tanh(e) \tag{7}$$

where e is the position error, and y is the output of the tanh function. A plot of this function is shown in Figure 55. The output of the PD controller with feedforward and nonlinear compensation is given by equation 8.

$$u = bias + k_t \tanh(ae) + k_p e + k_d \frac{de}{dt} \tag{8}$$

Where k_t is the tanh gain, and a is a gain on the argument of the tanh function.

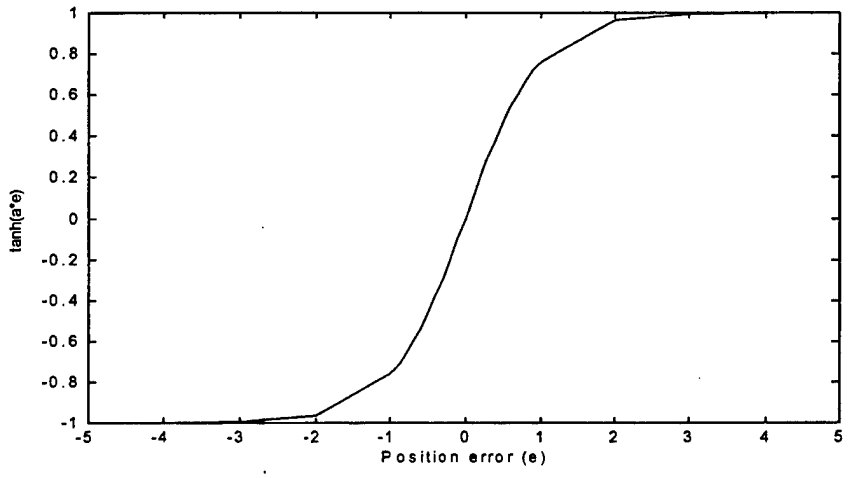

Figure 55. Plot of the tanh function

If the position error is between negative one and zero, the output of the tanh function is negative, and the saturation function outputs a zero. This occurs when the actual position is less than, or equal to, the ordered position. If the position error is between zero and positive one, the output of the tanh function is proportional to the position error. If the position error is greater than one, the output of the tanh function is one. Therefore, the tanh function operates as a large gain when the position error is small, and a small gain when the position error is large. Also by varying the gain a, the

operation of the tanh function about the origin can be controlled (see Figure 56). This provides for a faster response without overshoot.

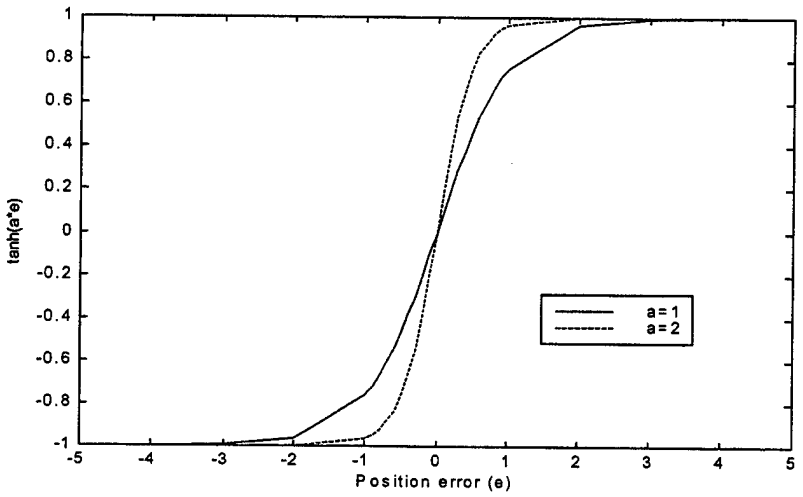

Figure 56. Effects of varying the tanh gain a.

Several experiments were conducted with the PD control with the non-linear control using various values of tanh gain. The tanh gain is a gain on the output of the tanh function. All experiments were conducted for a 3.5mm displacement, with a proportional gain and derivative gain of 20, and a maximum actuation current of 1.5 amps. The results are shown in Figures 57 - 59.

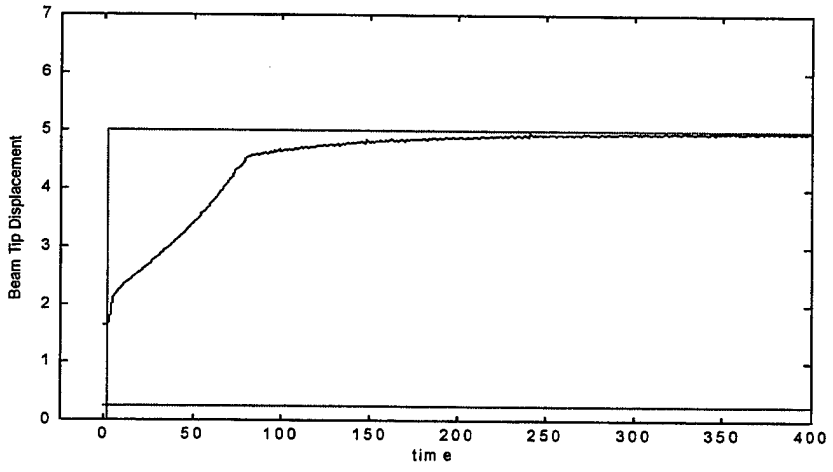

Figure 57. tanh gain = 5

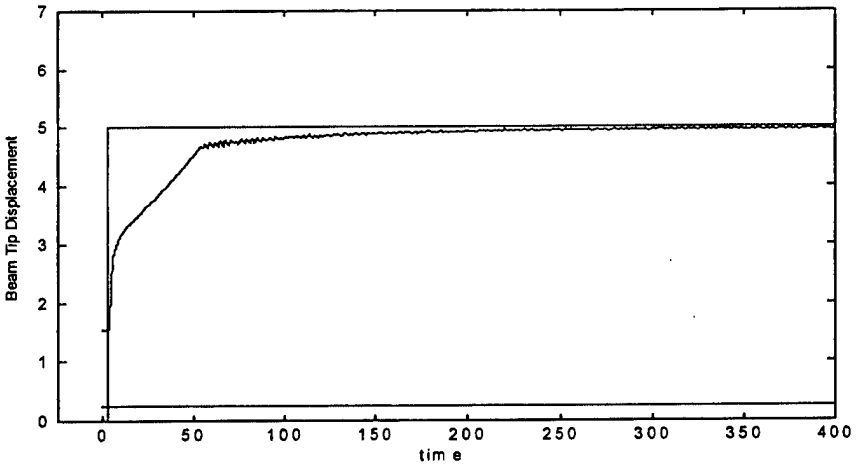

Figure 58. tanh gain = 10

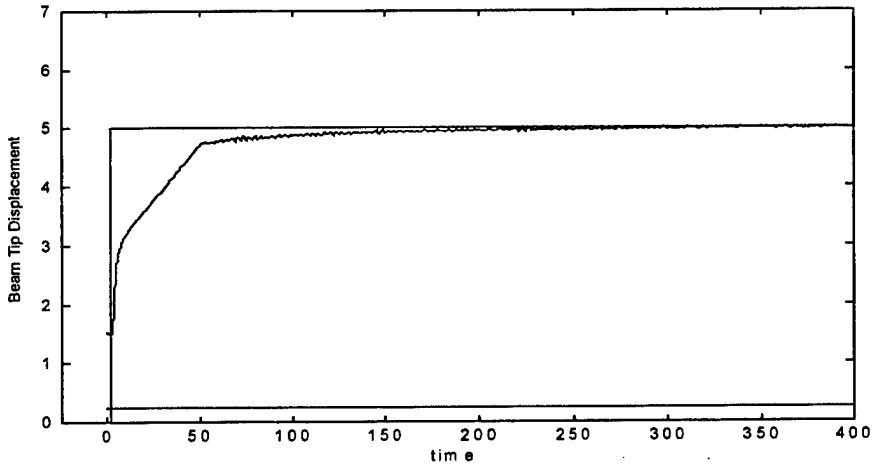

Figure 59. tanh gain = 15

It can be seen that by adding a non-linear compensator, the settling was reduced from approximately 300 seconds to approximately 150 seconds.

VI. CONCLUSION AND RECOMMENDATION

A. CONCLUSION

The shape memory alloy composite beam experiment successfully demonstrated that shape memory alloy actuators can precisely control the position of a composite beam. The PD control with feed-forward compensation and PD control with non-linear feedforward compensation provided control within 0.05 mm of the desired position. Although precision control was achieved, active position control is in one direction only. Additionally, future space applications will require precision shape control vice position control. Designing a more responsive control system will require the development of an analytical model of the SMA composite beam and analytical models are not available in the open literature. Developing this model is very difficult due to the non-linearity's of the SMA material. In order to achieve an accurate position control, feed-forward compensation was necessary. The feed-forward compensation was necessary to compensate for the heat loss. Estimating the feed-forward compensation can become a problem as the satellite temperature varies significantly.

B. RECOMMEDATION

This is the first step in determining the feasibility of using SMA materials for antenna shape control at the NPS Spacecraft Research and Design Center. The SMA beam tip position control is very good with a constant bias voltage. This bias voltage (feed-forward compensator) was added to compensate for the heat loss from the SMA material and reduce the position error. The bias voltage was actually unique to the desired position; therefore, a bias voltage for a given position may not be the ideal bias voltage for another desired position, because the resistance of the SMA actuators change as the material undergoes phase transformation from martensite to austenite. The bias voltage must be automated, or automatically updated for the change in resistance. Additionally, the proportional, derivative and non-linear gains should be tuned for optimal control. This optimal control could be to minimize position error, response time,

or even to minimize power consumption. In addition, strain gauges should be incorporated into the SMA beam in order to perform shape control. Also, a higher precision control could be accomplished by placing SMA actuators on both faces of the beam, or possibly by constructing a composite parabolic dish with actuators on both the outside and inside faces. This would provide maximum flexibility for shape control, and would show conclusively that antenna shape control using shape memory alloys is feasible. Finally, an analytical model must be developed in order to accurately predict the behavior of the shape memory alloy beam.

REFERENCES

Adler A, Mikulas M M, Hedgepeth J M, Stallard M, and Garnham J "Novel Phased Array Antenna Structure Design".

Bhattacharyya A, Lagoudas D C, Wang Y, and Kinra V K "On the role of thermoelectric heat transfer in the design of SMA actuators: theorectical modeling and experiment" IOP Publishing Ltd. 1995

Chen C T, "Analog and Digital Control System Design: Transfer-Function, State-Space, and Algebraic Methods" Saunders College Publishing 1993

Hurlbut B J, and Regelbrugge M E, "Evaluation of a Constitutive Model for Shape Memory Alloys Embedded in Shell Structures" Journal of Reinforced Plastics and Composites, vol 15. 1996

Maclean B J, Patterson G J, Draper J L, Carpenter B F, and Misra M S "Shape Memory Material Actuator (SMMA)". Martin Marietta Astronautics Group 1991

McNichols J L, and Cory J S, "Thermodynamics of Nitinol", Journal of Applied Physics, Vol 61 No. 3 1987

Otsuka K, and Wayman C M, "Shape Memory Materials", Cambridge University Press 1998

Product Literature, "Properties of NiTi" 1995

Slotine J J, and Li W, "Applied Nonlinear Control" Prentice-Hall Inc. 1991

Shu S G, Lagoudas D C, Hughes D, and Wen J T "Modeling of a flexible beam actuated by shape memory alloy wires". IOP Publishing Ltd. 1997

Tabata M, and Natori M C, "Active Shape Control of a Deployable Space Antenna Reflector", Journal of Intelligent Material Systems and Structures, Vol. 7 1996

Waram T, "Actuator Design Using Shape Memory Alloys" 1993

INITIAL DISTRIBUTION LIST

1. Defense Technical Information Center.....2
   8725 John J. Kingman Road, Suite 0944
   Ft. Belvoir, VA 22060-6218

2. Dudley Knox Library.....2
   Naval Postgraduate School
   411 Dyer Road
   Monterey, CA 93943-5002

3. Chairman, Code AA.....1
   Department of Aeronautics and Astronautics
   Naval Postgraduate School
   Monterey, CA 93943

4. Professor Brij N. Agrawal, Code AA/Ag.....2
   Department of Aeronautics and Astronautics
   Naval Postgraduate School
   Monterey, CA 93943

5. Dr. Gangbing Song, Assistant Professor.....1
   Department of Mechanical Engineering
   The University of Akron
   Akron, OH 44325-3903

6. LT Brian L. Kelly, USN.....4
   1460 North Oak Hill Rd.
   Litchfield, ME 04350